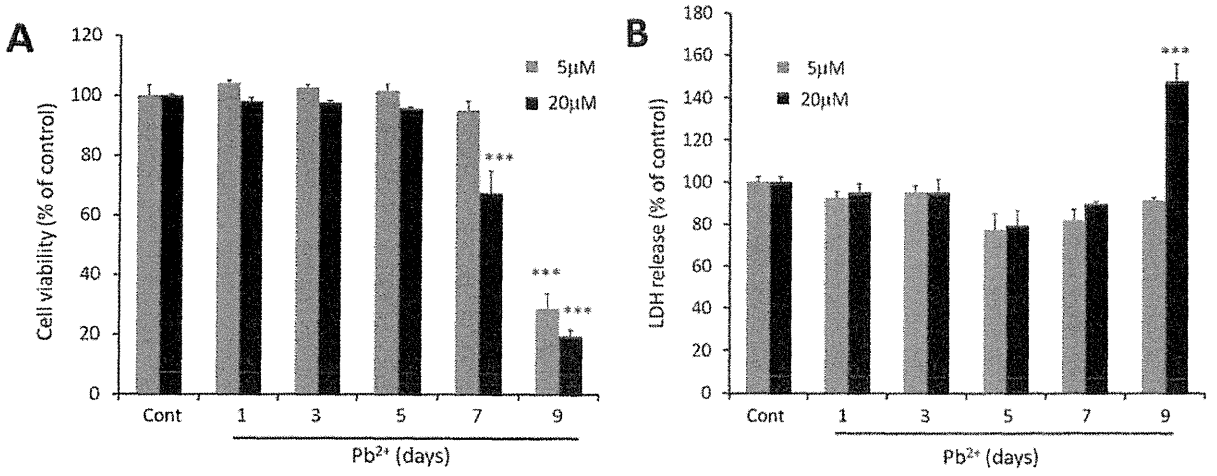

Fig. 1. Influence of long-term exposure to lead acetate (Pb^{2+}) on neurotoxicity. Cortical neurons were exposed to 5 and 20 μM Pb^{2+} for 1-9 days. Then cell viability was measured by means of trypan blue assay (A) and LDH assay (B). Data are expressed as mean + S.E.M. (n = 4). ***P < 0.001 vs. Cont.

exposure to 20 μM lead for 7 and 9 days decreased the cell viability to 67% and 19% of the control, respectively (Fig. 1A). Moreover, LDH release from cortical neurons was increased to 147% of the control after exposure to 20 μM lead for 9 days, although exposure to 5 μM lead had no effect (Fig. 1B).

Effect of long-term exposure of lead on GluR2 expression

We hypothesized that long-term exposure to lead would also decrease GluR2 expression, and would result in neuronal cell death. To examine this hypothesis, cortical neurons were exposed to 0.1-100 μM lead for 9 days and GluR2 protein expression was measured. As shown in Fig. 2A, a concentration-dependent decrease of GluR2 expression was seen upon exposure of the neurons to lead at concentrations above 1 μM and the decrease reached statistical significance at 5 μM. In 100 μM lead exposure, β-actin expression was also decreased, maybe due to drastic cell death (Fig. 2A). Moreover, cortical neurons were exposed to 5 and 20 μM lead for 1-9 days. A time-dependent decrease of GluR2 expression was observed in the neurons exposed to 5 and 20 μM lead. Exposure to 5 μM lead for 7 and 9 days significantly decreased the expression of GluR2 to 50% and 29% of the control (Fig. 2B), while exposure to 20 μM lead for 7 and 9 days significantly decreased the expression of GluR2 to 35% and 30% of the control (Fig. 2C). GluR2 subunits are largely expressed in cytoplasm, but some of them are expressed in plasma membrane and act as components of AMPA receptors. Next, GluR2 expression at the plasma membrane was examined by immunocytochemistry (Fig. 3). Membrane expression of GluR2, which was confirmed by co-localization with N-cadherin, a membrane protein marker, was observed in the control cells. Exposure to 5 and 20 μM lead for 9 days markedly decreased GluR2 expression, in accordance with the result of western blotting (Fig. 2). Moreover, co-localization of GluR2 and N-cadherin was also considerably reduced, while intracellular distribution of GluR2 was not altered in these cells. These results suggest that exposure to lead decreases GluR2 expression, leading to a decrease in plasma membrane GluR2.

Amelioration of lead-induced GluR2 reduction and neuronal cell death by BDNF

It has been reported that BDNF potently induces GluR2 promoter activity in SH-SY5Y cells, resulting in increased expression of GluR2 protein (Brené *et al.*, 2000). Thus, we tested whether BDNF also increased GluR2 protein expression in cortical neurons and ameliorated lead-induced neuronal cell death. Although the GluR2 protein level was not increased, the decrease of GluR2 expression induced by exposure to 5 and 20 μM lead was partly reversed by 50 ng/ml BDNF (Fig. 4A). Concomitantly, the decrease of cell viability caused by exposure to 5 and 20 μM lead was also significantly ameliorated by 50 ng/ml BDNF (Fig. 4B).

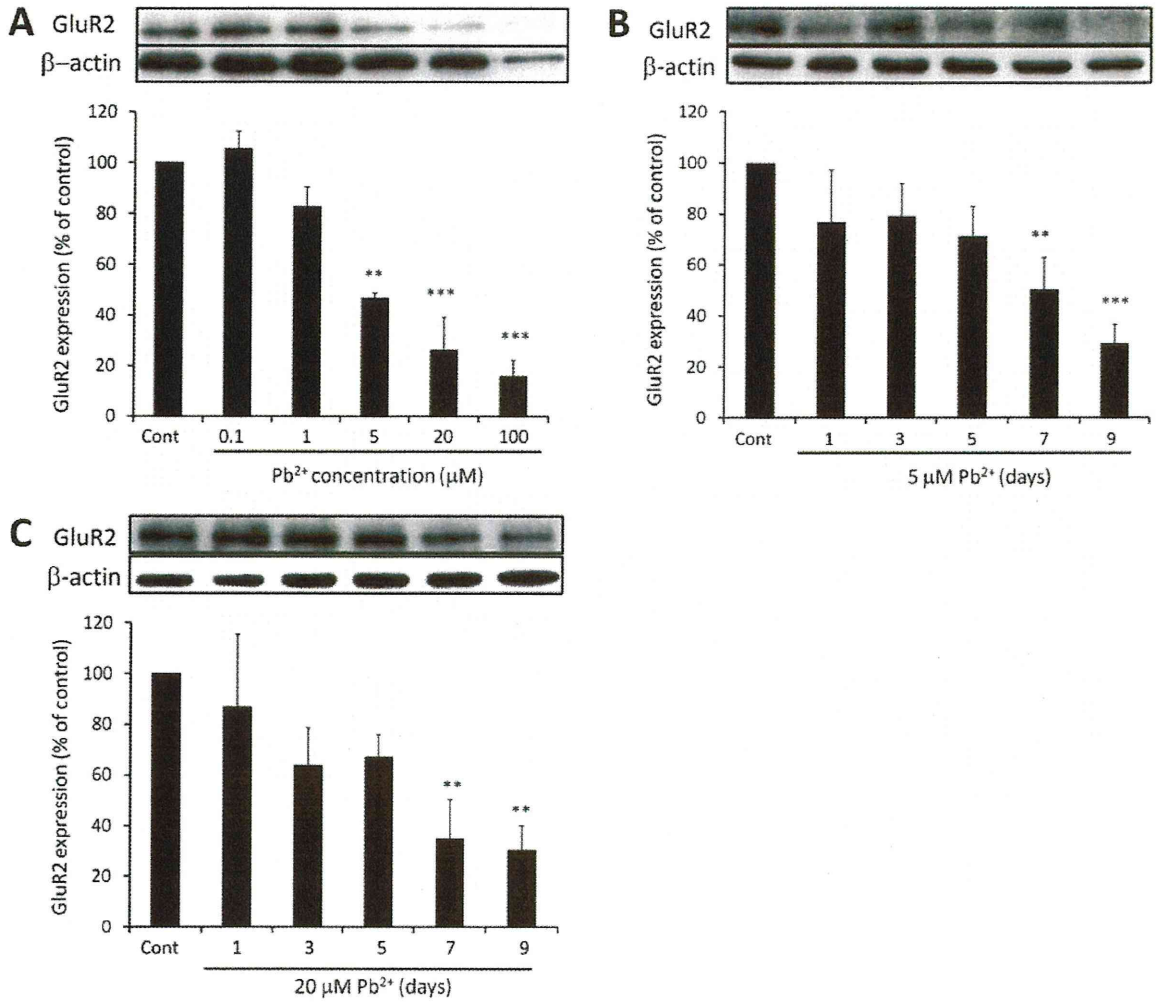

Fig. 2. Change of GluR2 protein expression induced by Pb^{2+}. Cortical neurons were exposed to 0.1-100 μM Pb^{2+} for 9 days (A), 5 μM Pb^{2+} for 1-9 days (B) and 20 μM (C) Pb^{2+} for 1-9 days, then GluR2 protein was detected by western blotting. Quantitative analysis was performed with Image J software and GluR2 protein levels were corrected on the basis of β-actin protein levels. Data are expressed as mean + S.E.M. (n = 3) **P < 0.01 vs. cont, ***P < 0.001 vs. cont.

DISCUSSION

In this study, cultured rat cortical neurons were exposed to lead to test our hypothesis that lead induces a decrease of GluR2 expression that in turn promotes neuronal cell death. We found that exposure to lead at 5-20 μM for 9 days decreased cell viability (Fig. 1A) and LDH release was increased after exposure to 20 μM lead for 9 days (Fig. 1B). Trypan blue-stained cells are regarded as dead, whereas LDH assay measures LDH release from membrane-disrupted cells. Thus, the differences in evaluation of neuronal cell death between trypan blue assay and LDH assay is considered to be due to the different endpoints used to determine cell death in the two assays.

The expression of GluR2, an AMPA-type glutamate receptor subunit, was significantly decreased by exposure to 5-20 μM lead for 7 days (Fig. 2). It was reported that exposure to 0.1-10 μM lead for 48 hr decreased cell proliferation and increased caspase-3 activity in human SH-SY5Y neuroblastoma cells (Chetty *et al.*, 2005). Shinkai *et al.* (2010) reported that 5 μM lead induces endoplasmic

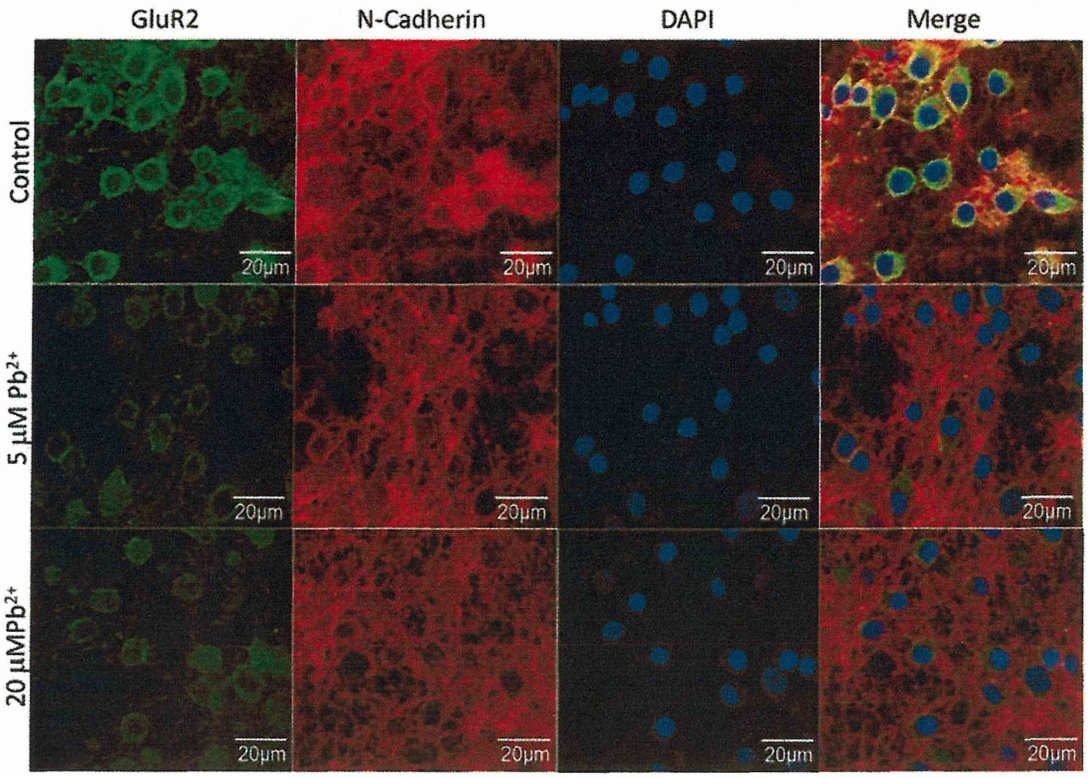

Fig. 3. Change of GluR2 protein expression on the plasma membrane induced by Pb^{2+}. Cortical neurons were exposed to 5 and 20 μM Pb^{2+} for 9 days, and immunocytochemical staining was performed using a mouse anti-GluR2 antibody that recognizes the N-terminal extracellular domain of GluR2 (green) and a rabbit anti-N-cadherin antibody (red). Nuclear staining was performed using DAPI (blue). Yellow indicates colocalization between GluR2 and N-cadherin.

reticulum chaperones GRP78 and GRP94 via JNK-AP-1 pathway in vascular endothelial cells. Thus, the lead concentrations used in this study are similar to those used in other studies on the *in vitro* toxicities of lead. Incidentally, lead concentrations of up to 5 μM in blood have been reported in workers exposed to lead (Tomokuni *et al.*, 1993). It is well known that lead induces hematotoxicity by inhibiting the activity of enzymes involved in heme biosynthesis such as δ-aminolevulinic acid dehydratase. It is believed to be the most sensitive to lead (Bottomley and Muller-Eberhard, 1988). However, δ-aminolevulinic acid dehydratase is inhibited only in the presence of comparatively high lead concentrations of 0.1-1 mM in human erythroblastic cultures (Rio *et al.*, 2001). Thus, the concentrations used in this study are lower than those used in the above studies.

We have reported that long-term exposure of rat cortical neurons to tributyltin (TBT) decreases GluR2 expression, which results in increased Ca^{2+} permeability of AMPA receptors, because the Ca^{2+} permeability of AMPA receptors depends on whether or not they contain the GluR2 subunit (Nakatsu *et al.*, 2009). It was reported that GluR2 knockdown rats showed neuronal cell death in hippocampal CA1 and CA3, and the neuronal cell death was reduced by injection of Naspm (an open channel blocker selective for Ca^{2+}-permeable, GluR2-lacking AMPA receptors) and CNQX (a competitive blocker of AMPA receptors) (Oguro *et al.*, 1999), which suggests that GluR2 knockdown-induced neuronal cell death was mediated by Ca^{2+}-permeable, GluR2-lacking AMPA receptors. It has also been reported that knockdown of GluR2 exacerbates kainate-induced neuronal death (Friedman and Velísková, 1998; Friedman *et al.*, 2003). Iihara *et al.* (2001) suggested that kainate-induced neuronal cell death in GluR2 knockdown animals involves altered Na^{2+} permeability as well as altered Ca^{2+} permeability. It

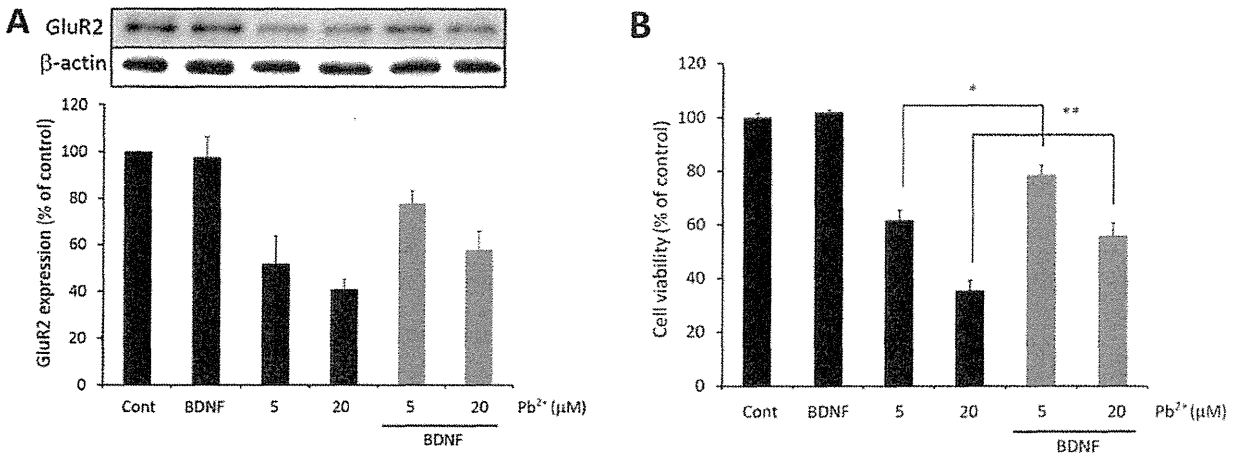

Fig. 4. Influence of exposure to BDNF on Pb^{2+}-induced decrease of GluR2 and neuronal cell death. Cortical neurons were exposed to 5 and 20 μM Pb^{2+} with or without 50 ng/ml BDNF for 9 days. (A) GluR2 protein was detected by western blotting. Quantitative analysis was performed with Image J software and GluR2 protein levels were corrected on the basis of β-actin protein levels. Data are expressed as mean + S.E.M. (n = 4-5). (B) Cell viability was measured by means of trypan blue assay. Data are expressed as mean + S.E.M. (n = 8). *P < 0.05, **P < 0.01.

is known that GluR2 knockdown mice also show behavioral changes, such as impaired novelty-induced exploratory activities, disrupted motor coordination, and reduced self-directed behaviors, compared with control mice (Jia *et al.*, 1996). These findings are consistent with the idea that lead-induced GluR2 decrease can induce neuronal death via the increase of Ca^{2+} permeability of AMPA receptors. However, further studies are needed to measure lead-induced Ca^{2+} entry into neurons.

Expression of GluR2 can be induced by BDNF (Brené *et al.*, 2000), and one of the neuroprotective effects of BDNF is supposed to be mediated by recovery of GluR2. We also investigated whether increasing GluR2 expression by exposure to BDNF results in amelioration of lead-induced neuronal cell death. We found that the lead-induced GluR2 decrease was partly reversed and neuronal cell viability was increased by exposure to 50 ng/ml BDNF (Fig. 4). Because GluR2 levels are thought to reach plateau in primary cortical neurons, BDNF may not increase basal GluR2 expression. These results support the hypothesis that lead causes neuronal cell death through decreasing GluR2 protein expression, though BDNF might rescue lead-induced neuronal death by other mechanism such as an activation of PI3-kinase-Akt pathway (Hetman *et al.*, 1999). It should be confirmed that GluR2 overexpression recovers cell viability decreased by lead.

In conclusion, we investigated the influence of long-term lead exposure on cultured cortical neurons. Lead induced a decrease of GluR2 protein and caused neuronal cell death. The decrease of GluR2 expression was considered to cause the lead-induced neuronal cell death, because cell viability was restored by BDNF treatment, which elicits a recovery of GluR2. A decrease in the population of GluR2-containing AMPA receptors is associated with increased Ca^{2+} influx. Our findings raise the possibility that GluR2 decrease in the brain is involved in lead-induced *in vivo* neurotoxicity, disorder of behavior, and impairment of cognitive function.

ACKNOWLEDGMENT

We thank the Analysis Center of Life Science, Hiroshima University for the use of their facilities. This work was supported by JSPS KAKENHI Grant Number 23310047 (to Y. Kotake).

REFERENCES

Alkondon, M., Costa, A.C., Radhakrishnan, V., Aronstam, R.S. and Albuquerque, E.X. (1990): Selective blockade of NMDA-activated channel currents may be implicated in learning deficits caused by lead. FEBS Lett., **261**, 124-130.

Bellinger, D., Leviton, A., Allred, E. and Rabinowitz, M. (1994): Pre- and postnatal lead exposure and behavior problems in school-aged children. Environ. Res., **66**, 12-30.

Blandini, F., Porter, R.H. and Greenamyre, J.T. (1996): Glutamate

and Parkinson's disease. Mol. Neurobiol., **12**, 73-94.
Bottomley, S.S. and Muller-Eberhard, U. (1988): Pathophysiology of heme synthesis. Semin. Hematol., **25**, 282-302.
Brené, S., Messer, C., Okado, H., Hartley, M., Heinemann, S.F. and Nestler, E.J. (2000): Regulation of GluR2 promoter activity by neurotrophic factors via a neuron-restrictive silencer element. Eur. J. Neurosci., **12**, 1525-1533.
Canfield, R.L., Gendle, M.H. and Cory-Slechta, D.A. (2004): Impaired neuropsychological functioning in lead-exposed children. Dev. Neuropsychol., **26**, 513-540.
Chetty, C.S., Vemuri, M.C., Campbell, K. and Suresh, C. (2005): Lead-induced cell death of human neuroblastoma cells involves GSH deprivation. Cell. Mol. Biol. Lett., **10**, 413-423.
Choi, D.W. (1988): Calcium-mediated neurotoxicity: relationship to specific channel types and role in ischemic damage. Trends Neurosci., **11**, 465-469.
Friedman, L.K., Segal, M. and Velísková, J. (2003): GluR2 knockdown reveals a dissociation between [Ca2+]i surge and neurotoxicity. Neurochem. Int., **43**, 179-189.
Friedman, L.K. and Velísková, J. (1998): GluR2 hippocampal knockdown reveals developmental regulation of epileptogenicity and neurodegeneration. Brain Res. Mol. Brain Res., **61**, 224-231.
Froehlich, T.E., Lanphear, B.P., Auinger, P., Hornung, R., Epstein, J.N., Braun, J. and Kahn, R.S. (2009): Association of tobacco and lead exposures with attention-deficit/hyperactivity disorder. Pediatrics, **124**, e1054-e1063.
Gavazzo, P., Zanardi, I., Baranowska-Bosiacka, I. and Marchetti, C. (2008): Molecular determinants of Pb2+ interaction with NMDA receptor channels. Neurochem. Int., **52**, 329-337.
Gracia, R.C. and Snodgrass, W.R. (2007): Lead toxicity and chelation therapy. Am. J. Health Syst. Pharm., **64**, 45-53.
Guilarte, T.R., McGlothan, J.L. and Nihei, M.K. (2000): Hippocampal expression of N-methyl-D-aspartate receptor (NMDAR1) subunit splice variant mRNA is altered by developmental exposure to Pb(2+). Brain Res. Mol. Brain Res., **76**, 299-305.
Hashida, T., Kotake, Y. and Ohta, S. (2011): Protein disulfide isomerase knockdown-induced cell death is cell-line-dependent and involves apoptosis in MCF-7 cells. J. Toxicol. Sci., **36**, 1-7.
Hetman, M., Kanning, K., Cavanaugh, J.E. and Xia, Z. (1999): Neuroprotection by brain-derived neurotrophic factor is mediated by extracellular signal-regulated kinase and phosphatidylinositol 3-kinase. J. Biol. Chem., **274**, 22569-22580.
Hirasawa, T., Wada, H., Kohsaka, S. and Uchino, S. (2003): Inhibition of NMDA receptors induces delayed neuronal maturation and sustained proliferation of progenitor cells during neocortical development. J. Neurosci. Res., **74**, 676-687.
Hollmann, M. and Heinemann, S. (1994): Cloned glutamate receptors. Annu. Rev. Neurosci., **17**, 31-108.
Iihara, K., Joo, D.T., Henderson, J., Sattler, R., Taverna, F.A., Lourensen, S., Orser, B.A., Roder, J.C. and Tymianski, M. (2001): The influence of glutamate receptor 2 expression on excitotoxicity in Glur2 null mutant mice. J. Neurosci., **21**, 2224-2239.
Jia, Z., Agopyan, N., Miu, P., Xiong, Z., Henderson, J., Gerlai, R., Taverna, F.A., Velumian, A., MacDonald, J., Carlen, P., Abramow-Newerly, W. and Roder, J. (1996): Enhanced LTP in mice deficient in the AMPA receptor GluR2. Neuron, **17**, 945-956.
Kjøller, C. and Diemer, N.H. (2000): GluR2 protein synthesis and metabolism in rat hippocampus following transient ischemia and ischemic tolerance induction. Neurochem. Int., **37**, 7-15.
Kondo, M., Sumino, R. and Okado, H. (1997): Combinations of AMPA receptor subunit expression in individual cortical neurons correlate with expression of specific calcium-binding proteins. J. Neurosci., **17**, 1570-1581.
Laidlaw, M.A., Mielke, H.W., Filippelli, G.M., Johnson, D.L. and Gonzales, C.R. (2005): Seasonality and children's blood lead levels: developing a predictive model using climatic variables and blood lead data from Indianapolis, Indiana, Syracuse, New York, and New Orleans, Louisiana (USA). Environ. Health Perspect., **113**, 793-800.
Lanphear, B.P., Hornung, R., Khoury, J., Yolton, K., Baghurst, P., Bellinger, D.C., Canfield, R.L., Dietrich, K.N., Bornschein, R., Greene, T., Rothenberg, S.J., Needleman, H.L., Schnaas, L., Wasserman, G., Graziano, J. and Roberts R. (2005): Low-level environmental lead exposure and children's intellectual function: an international pooled analysis. Environ. Health Perspect., **113**, 894-899.
Leviton, A., Bellinger, D., Allred, E.N., Rabinowitz, M., Needleman, H. and Schoenbaum, S. (1993): Pre- and postnatal low-level lead exposure and children's dysfunction in school. Environ. Res., **60**, 30-43.
Links, J.M., Schwartz, B.S., Simon, D., Bandeen-Roche, K. and Stewart, W.F. (2001): Characterization of toxicokinetics and toxicodynamics with linear systems theory: application to lead-associated cognitive decline. Environ. Health Perspect., **109**, 361-368.
Liu, S.J. and Zukin, R.S. (2007): Ca2+-permeable AMPA receptors in synaptic plasticity and neuronal death. Trends Neurosci., **30**, 126-134.
Luo, T., Wu, W.H. and Chen, B.S. (2011): NMDA receptor signaling: death or survival? Front Biol., **6**, 468-476.
Lustberg, M. and Silbergeld, E. (2002): Blood lead levels and mortality. Arch. Intern. Med., **162**, 2443-2449.
Monti, B., Marri, L. and Contestabile, A. (2002): NMDA receptor-dependent CREB activation in survival of cerebellar granule cells during *in vivo* and *in vitro* development. Eur. J. Neurosci., **16**, 1490-1498.
Nakatsu, Y., Kotake, Y., Takishita, T. and Ohta, S. (2009): Long-term exposure to endogenous levels of tributyltin decreases GluR2 expression and increases neuronal vulnerability to glutamate. Toxicol. Appl. Pharmacol., **240**, 292-298.
Neal, A.P., Worley, P.F. and Guilarte, T.R. (2011): Lead exposure during synaptogenesis alters NMDA receptor targeting via NMDA receptor inhibition. Neurotoxicology, **32**, 281-289.
Nihei, M.K., Desmond, N.L., McGlothan, J.L., Kuhlmann, A.C. and Guilarte, T.R. (2000): N-methyl-D-aspartate receptor subunit changes are associated with lead-induced deficits of long-term potentiation and spatial learning. Neuroscience, **99**, 233-242.
Oguro, K., Oguro, N., Kojima, T., Grooms, S.Y., Calderone, A., Zheng, X., Bennett, M.V. and Zukin, R.S. (1999): Knockdown of AMPA receptor GluR2 expression causes delayed neurodegeneration and increases damage by sublethal ischemia in hippocampal CA1 and CA3 neurons. J. Neurosci., **19**, 9218-9227.
Rio, B., Froquet, R. and Parent-Massin, D. (2001): In vitro effect of lead acetate on human erythropoietic progenitors. Cell. Biol. Toxicol., **17**, 41-50.
Shinkai, Y., Yamamoto, C. and Kaji, T. (2010): Lead induces the expression of endoplasmic reticulum chaperones GRP78 and GRP94 in vascular endothelial cells via the JNK-AP-1 pathway. Toxicol. Sci., **114**, 378-386.
Tomokuni, K., Ichiba, M. and Fujishiro, K. (1993): Interrelation between urinary delta-aminolevulinic acid (ALA), serum ALA,

and blood lead in workers exposed to lead. Ind. Health, **31**, 51-57.

Tymianski, M. (1996): Cytosolic calcium concentrations and cell death *in vitro*. Adv. Neurol., **71**, 85-105.

Ying, H.S., Weishaupt, J.H., Grabb, M., Canzoniero, L.M., Sensi, S.L., Sheline, C.T., Monyer, H. and Choi, D.W. (1997): Sublethal oxygen-glucose deprivation alters hippocampal neuronal AMPA receptor expression and vulnerability to kainate-induced death. J. Neurosci., **17**, 9536-9544.

Metallomics

RSC Publishing

PAPER

AMP-activated protein kinase-mediated glucose transport as a novel target of tributyltin in human embryonic carcinoma cells†

Cite this: DOI: 10.1039/c3mt20268b

Shigeru Yamada,[a] Yaichiro Kotake,[b] Yuko Sekino[a] and Yasunari Kanda*[a]

Organotin compounds such as tributyltin (TBT) are known to cause various forms of cytotoxicity, including developmental toxicity and neurotoxicity. However, the molecular target of the toxicity induced by nanomolar levels of TBT has not been identified. In the present study, we found that exposure to 100 nM TBT induced growth arrest in human pluripotent embryonic carcinoma cell line NT2/D1. Since glucose provides metabolic energy, we focused on the glycolytic system. We found that exposure to TBT reduced the levels of both glucose-6-phosphate and fructose-6-phosphate. To investigate the effect of TBT exposure on glycolysis, we examined glucose transporter (GLUT) activity. TBT exposure inhibited glucose uptake *via* a decrease in the level of cell surface-bound GLUT1. Furthermore, we examined the effect of AMP-activated protein kinase (AMPK), which is known to regulate glucose transport by facilitating GLUT translocation. Treatment with the potent AMPK activator, AICAR, restored the TBT-induced reduction in cell surface-bound GLUT1 and glucose uptake. In conclusion, these results suggest that exposure to nanomolar levels of TBT causes growth arrest by targeting glycolytic systems in human embryonic carcinoma cells. Thus, understanding the energy metabolism may provide new insights into the mechanisms of metal-induced cytotoxicity.

Received 28th December 2012,
Accepted 20th February 2013

DOI: 10.1039/c3mt20268b

www.rsc.org/metallomics

Introduction

Growing evidence suggests that environmental metals contribute to developmental toxicity and neurotoxicity.[1–3] Since the developing brain is inherently more vulnerable to injury than the adult brain, exposure to metals during early fetal development can potentially cause neurological disorders at doses much lower than those that are toxic in adults.[4–7] Therefore, it is necessary to elucidate the cytotoxic effects of such metals at low levels.

Organotin compounds are well known to cause cytotoxicity. Although organotin compounds or derivatives have been shown to have a potential anti-tumor activity[8,9] and some of them have already been entered into preclinical trials,[10] tributyltin (TBT) is considered to be associated with developmental toxicity and neurotoxicity.[11] For example, TBT can cause increased fetal mortality, decreased fetal birth weights, and behavioral abnormalities in rat offspring.[12,13] TBT is known to affect fertilization and embryonic development.[14] Moreover, TBT has been shown to induce neuronal death by glutamate excitotoxicity in cultured rat cortical neurons.[15] Although the use of TBT has already been restricted, butyltin compounds, including TBT, have been reported to be still present at concentrations between 50 and 400 nM in human blood.[16] However, the mechanism by which nanomolar levels of TBT cause cytotoxicity is not fully understood.

Glucose is the primary energy source for homeostasis. Glucose transport across the plasma membrane *via* a glucose transporter (GLUT) is a rate-limiting step in glucose metabolism.[17] AMP-activated protein kinase (AMPK), a serine threonine kinase, has been shown to regulate glucose uptake by facilitating the translocation of the GLUT to the membrane or by activation of transporter activity at the plasma membrane.[18,19] The fetal brain has been reported to rely on anaerobic glycolysis to meet its energy demands.[20] Thus, GLUT is considered essential in the early organogenesis period. GLUT1, a major subtype of GLUT in fetal tissue, has been shown to mediate organogenesis in rat embryos.[21] In addition, clinical data regarding human GLUT1 deficiency syndrome suggest that GLUT1 is necessary for human brain development.[22]

In the present study, we hypothesized a possible link between TBT toxicity and glucose metabolism. We found that

[a] *Division of Pharmacology, National Institute of Health Sciences, 1-18-1, Kamiyoga, Setagaya-ku 158-8501, Japan. E-mail: kanda@nihs.go.jp; Fax: +81-3-3700-9704; Tel: +81-3-3700-9704*

[b] *Department of Xenobiotic Metabolism and Molecular Toxicology, Graduate School of Biomedical and Health Sciences, Hiroshima University, Japan*

† Electronic supplementary information (ESI) available. See DOI: 10.1039/c3mt20268b

exposure to TBT reduced the amounts of glucose-6-phosphate and fructose-6-phosphate *via* a decrease in surface-bound GLUT1 in the human pluripotent embryonic carcinoma cell line NT2/D1. In addition, treatment with the potent AMPK activator, 5-aminoimidazole-4-carboxyamide ribonucleoside (AICAR), restored the inhibitory effect of TBT on both cell surface-bound GLUT1 levels and glucose uptake. We report here that the glycolytic pathway is a molecular target of nanomolar levels of TBT in human embryonic carcinoma cells.

Methods

Cell culture

NT2/D1 cells were obtained from the American Type Culture Collection. The cells were cultured in Dulbecco's modified Eagle's medium (DMEM; Sigma-Aldrich, St. Louis, MO, USA) supplemented with 10% fetal bovine serum (FBS; Biological Industries, Ashrat, Israel) and 0.05 mg mL^{-1} penicillin–streptomycin mixture (Life Technologies, Carlsbad, CA, USA) at 37 °C and 5% CO_2. For neural differentiation, all-trans retinoic acid (RA; Sigma-Aldrich) was added to the medium twice a week at a final concentration of 10 μM.

Cell proliferation assay

Cell viability was measured using the CellTiter 96 AQueous One Solution Cell Proliferation Assay (Promega, Madison, WI, USA), according to the manufacturer's instructions. Briefly, NT2/D1 cells were seeded into 96-well plates and exposed to different concentrations of TBT. After exposure to TBT, One Solution Reagent was added to each well, and the plate was incubated at 37 °C for another 2 h. Absorbance was measured at 490 nm using an iMark microplate reader (Bio-Rad, Hercules, CA, USA).

Glucose uptake assay

A glucose uptake assay was performed using a fluorescent glucose derivative, 2-[*N*-(7-nitrobenz-2-oxa-1,3-diazol-4-yl)amino]-2-deoxy-D-glucose (2-NBDG; Peptide Institute Inc., Osaka, Japan) by the previously reported procedure with slight modifications.[23] Briefly, NT2/D1 cells exposed to TBT were incubated with 2-NBDG (100 μM) for 2 h at 37 °C. The 2-NBDG uptake reaction was stopped by draining the incubation medium and washing the cells twice with ice-cold PBS. The incorporated 2-NBDG was measured using a Wallac1420ARVO fluoroscan (Perkin-Elmer, Waltham, MA, USA) with excitation at 488 nm and emission at 515 nm. The fluorescence intensities were normalized to the total protein content.

Hexokinase activity assay

Hexokinase activity was determined using a commercial Hexokinase Colorimetric Assay Kit (Biovision, Mountain View, CA, USA), according to the manufacturer's instructions.

AMPK activity assay

AMPK activity was determined using a commercial CycLex AMP Kinase Assay Kit (MBL International, Woburn, MA, USA), according to the manufacturer's instructions.

Determination of glucose-6-phosphate and fructose-6-phosphate

Intracellular metabolites were extracted and used for subsequent capillary electrophoresis time-of-flight mass spectrometry (CE-TOFMS) analysis, as described previously.[24] Glucose-6-phosphate and fructose-6-phosphate were determined using an Agilent CE capillary electrophoresis system (Agilent Technologies, Waldbronn, Germany) equipped with an Agilent G3250AA LC/MSD TOF system (Agilent Technologies, Palo Alto, CA), an Agilent 1100 series isocratic HPLC pump, a G1603A Agilent CE-MS adapter kit, and a G1607A Agilent CE-electrospray ionization 53-MS sprayer kit. For system control and data acquisition, G2201AA Agilent ChemStation software was used for CE, and Agilent TOF (Analyst QS) software was used for TOFMS.

Western blotting

Western blotting was performed as previously reported.[25] Briefly, the cells were lysed using Cell Lysis Buffer (Cell Signaling Technology, Danvers, MA, USA), and proteins were then separated by sodium dodecyl sulfate (SDS)-polyacrylamide gel electrophoresis and electrophoretically transferred to Immobilon-P membranes (Millipore, Billerica, MA, USA). The membranes were probed using primary antibodies (anti-GLUT1 polyclonal antibodies [1 : 200; Santa Cruz Biotechnology, Santa Cruz, CA, USA], anti-c-Myc polyclonal antibodies [1 : 1000; Sigma-Aldrich], anti-Flag monoclonal antibodies [1 : 1000; Sigma-Aldrich], and anti-β-actin monoclonal antibodies [1 : 1000; Sigma-Aldrich]). The membranes were then incubated with secondary antibodies against rabbit or mouse IgG conjugated with horseradish peroxidase (Cell Signaling Technology). The bands were visualized using an ECL Western Blotting Analysis System (GE Healthcare, Buckinghamshire, UK), and images were acquired using a LAS-3000 Imager (Fujifilm UK Ltd., Systems, Bedford, UK). The density of each band was quantified with ImageJ software (NIH, Bethesda, MD, USA).

Cell surface biotinylation

NT2/D1 cell surface proteins were biotinylated using a Cell Surface Protein Isolation Kit, according to the manufacturer's instructions (Pierce, Rockford, IL, USA). Briefly, cells were incubated with ice-cold phosphate-buffered saline (PBS; pH 7.4) containing Sulfo-NHS-SS-Biotin, with gentle rocking for 30 min at 4 °C. The biotinylated proteins were precipitated with streptavidin beads and eluted from the beads with SDS sample buffer. The proteins were analyzed by western blotting with anti-GLUT1 antibodies.

Immunohistochemistry

Cells, cultured on glass coverslips, were fixed in 4% paraformaldehyde in PBS (pH 7.4) for 15 min at room temperature. The fixed cells were incubated with anti-GLUT1 polyclonal antibodies (1 : 100; Santa Cruz) for 1 h at room temperature. Finally, they were incubated with Alexa488-conjugated secondary antibodies (1 : 200; Life Technologies) for 1 h at room temperature. The cells were enclosed in SlowFade (Life Technologies) and examined under a BIOREVO BZ-9000 fluorescent microscope (Keyence, Osaka, Japan).

Transfection

Cells were transiently transfected with Flag-tagged GLUT1 in pEF6 (a kind gift from Dr Rathmell) and c-Myc-tagged constitutively active-AMPK-α1 (T172D) or c-Myc-tagged dominant-negative-AMPK-α1 (K45R) in pcDNA3 (a kind gift from Dr Carling) using the FuGene HD Transfection Reagent (Promega), according to the manufacturer's protocol. After 48 h incubation, the transfectants were cultured with 12.5 μg mL^{-1} blasticidin or 0.5 mg mL^{-1} G418.

Real-time PCR

After total RNA was isolated from NT2/D1 cells using TRIzol (Life Technologies), quantitative real-time reverse transcription (RT)-PCR with a QuantiTect SYBR Green RT-PCR Kit (QIAGEN, Valencia, CA, USA) was performed using an ABI PRISM 7900HT sequence detection system (Applied Biosystems, Foster City, CA, USA), as previously reported.[26] The relative changes in the amounts of transcripts in each sample were normalized using ribosomal protein L13 (RPL13) mRNA levels. The sequences of the primers used for real-time PCR analysis are as follows: GLUT1 (forward, 5′-CCAGCTGCCATTGCCGTT-3′; reverse, 5′-GACGTAGGGACCACACAGTTGC-3′), GLUT2 (forward, 5′-CACACAAGACCTGGAATTGACA-3′; reverse, 5′-CGGTCATCCAGTGGAACAC-3′), GLUT3 (forward, 5′-CAATGCTCCTGAGAAGATCATAA-3′; reverse, 5′-AAAGCGGTTGACGAAGAGT-3′), GLUT4 (forward, 5′-CTGGGCCTCACAGTGCTAC-3′; reverse, 5′-GTCAGGCGCTTCAGACTCTT-3′), nestin (forward, 5′-GGCAGCGTTGGAACAGAGGT-3′; reverse, 5′-CATCTTGAGGTGCGCCAGCT-3′), NeuroD (forward, 5′-GGAAACGAACCCACTGTGCT-3′; reverse, 5′-GCCACACCAAATTCGTGGTG-3′), Math1 (forward, 5′-GTCCGAGCTGCTACAAACG-3′; reverse, 5′-GTGGTGGTGGTCGCTTTT-3′), MAP2 (forward, 5′-CCAATGGATTCCCATACAGG-3′; reverse, 5′-CTGCTACAGCCTCAGCAGTG-3′), RPL13 (forward, 5′-CATCGTGGCTAAACAGGTACTG-3′; reverse, 5′-GCACGACCTTGAGGGCAGCC-3′).

Materials

TBT was obtained from Tokyo Chemical Industry (Tokyo, Japan). Tin acetate (TA), AICAR, and rosiglitazone were obtained from Sigma-Aldrich. All other reagents were of analytical grade and obtained from commercial sources.

Statistical analysis

All data were presented as mean ± S.D. ANOVA followed by a *post hoc* Tukey test was used to analyze data in Fig. 1–4. Unpaired Student's *t* test was used to analyze data in Fig. 5. A *p* value of less than 0.05 was considered significant.

Results

To examine the effect of TBT on the proliferation of human NT2/D1 embryonic carcinoma cells, we exposed the cells to different concentrations of TBT for 24 h and measured cell viability by MTT assay. Treatment with TBT reduced cell viability in a dose-dependent manner (Fig. 1A; 0.03–0.3 μM). We observed that almost all cells were detached from the culture dish at TBT concentrations of 300 nM and above. In contrast, the less toxic TA had little effect at any concentration (Fig. 1A–e). We performed time-course experiments with 100 nM TBT, and determined the cell number. Exposure to

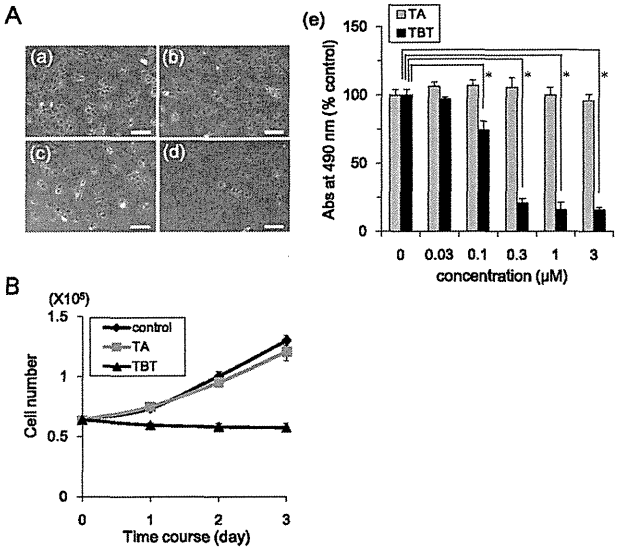

Fig. 1 Effect of TBT exposure on cell proliferation in NT2/D1 cells. (A) NT2/D1 cells were seeded into 96-well plates and exposed to TBT at different concentrations for 24 h. (a–d) Phase-contrast photomicrographs of NT2/D1 cells exposed to TBT at 0, 0.03, 0.1, or 0.3 μM (Bar = 100 μm). (e) Cell viability in the presence of TBT or TA was examined using the CellTiter 96 AQueous One Solution Cell Proliferation Assay. (B) NT2/D1 cells (6×10^5 cells) were seeded into 100 mm dishes and exposed to 100 nM TBT. After 24, 48, and 72 h, cell count was determined using a hemocytometer. *$P < 0.05$.

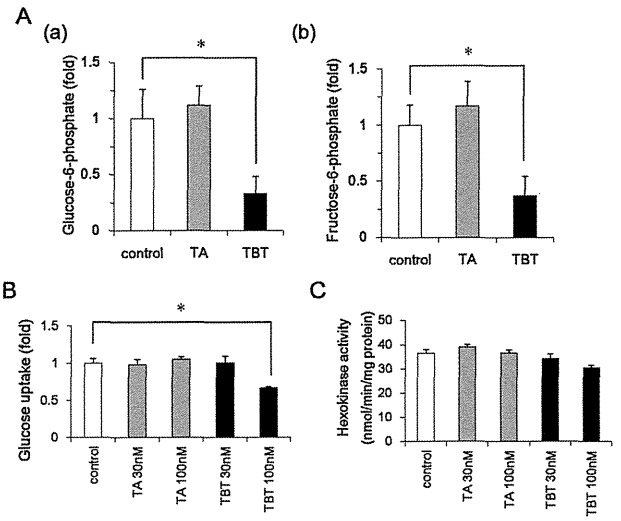

Fig. 2 Effect of TBT exposure on glycolytic systems in NT2/D1 cells. (A) After 24 h exposure to 100 nM TBT or TA, glucose 6-phosphate (a) and fructose 6-phosphate (b) levels were determined using CE-TOFMS. (B) After exposure to TBT or TA (30, 100 nM) for 24 h, glucose uptake assay was performed using a fluorescent glucose analog 2-NBDG. The fluorescence intensities of incorporated 2-NBDG were normalized to total cellular protein content. (C) After exposure to TBT or TA (30, 100 nM) for 24 h, hexokinase activity was measured using a commercial assay kit. *$P < 0.05$.

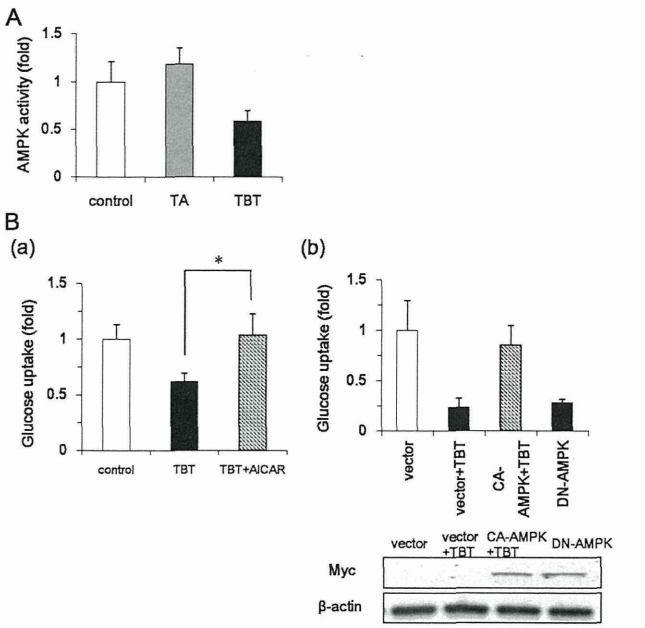

Fig. 3 Effect of AMPK on glucose uptake in NT2/D1 cells. (A) NT2/D1 cells were exposed to TBT or TA at 100 nM for 24 h. AICAR (0.5 mM) treatment was performed for 3 h. AMPK activity in the lysed cells was determined using a commercial assay kit. (B) NT2/D1 cells were exposed to TBT in the presence of 0.5 mM AICAR. (C) After overexpression of constitutively active (CA) mutants of AMPK, NT2/D1 cells were exposed to 100 nM TBT for 24 h, and glucose uptake assay was performed. After overexpression of dominant-negative (DN) mutants of AMPK, basal glucose uptake was tested. A glucose uptake assay was performed using the fluorescent glucose analog 2-NBDG. The fluorescence intensities of incorporated 2-NBDG were normalized to total cellular protein content. $^*P < 0.05$.

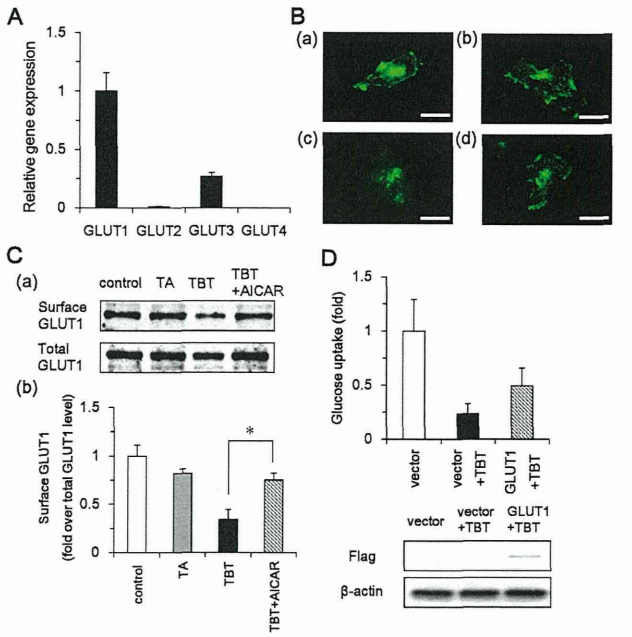

Fig. 4 Effect of TBT exposure on GLUT1 localization in NT2/D1 cells. (A) Expression of GLUT family by real-time PCR in NT2/D1 cells. Relative changes were determined by normalizing to RPL13. (B) After exposure to 100 nM TBT for 24 h, NT2/D1 cells were immunostained with anti-GLUT1 polyclonal antibodies. (a) Control, (b) 100 nM TA, (c) 100 nM TBT, and (d) 100 nM TBT + 0.5 mM AICAR. (Bar = 25 μm). (C) (a) NT2/D1 cell surface proteins were biotinylated using Sulfo-NHS-SS-Biotin, and then lysed. After precipitation with streptavidin beads, biotinylated proteins were analyzed by western blotting using anti-GLUT1 antibodies. Total GLUT1 protein was detected in cell lysate. (b) The relative density of bands was quantified with ImageJ software. Cell surface GLUT1 levels were normalized to total GLUT1 levels. (D) After overexpression of GLUT1, NT2/D1 cells were exposed to 100 nM TBT for 24 h, and glucose uptake assay was performed using the fluorescent glucose analog 2-NBDG. The fluorescence intensities of incorporated 2-NBDG were normalized to total cellular protein content. $^*P < 0.05$.

TBT suppressed the growth curve, but the total cell number did not alter throughout the time-course experiment (Fig. 1B). These data suggest that exposure to 100 nM TBT induced growth arrest in the cells without causing cell death.

Glucose provides metabolic energy for cell growth and it is incorporated by glucose transporters.[17] To examine the mechanism by which TBT induces growth arrest at low concentrations, we determined the glucose-6-phosphate, a major metabolite in glycolysis. We found that exposure to 100 nM TBT reduced the amount of glucose-6-phosphate (Fig. 2A). Fructose-6-phosphate, which is produced by isomerization of glucose 6-phosphate, also reduced by TBT. To check whether the decrease in glucose-6-phosphate is induced by inhibition of glucose transport, we examined the activity of glucose uptake by using 2-NBDG, a fluorescently labeled 2-deoxyglucose. Similar to the cell growth, glucose uptake was significantly inhibited by 100 nM TBT, not by 30 nM TBT (Fig. 2B). TA had little effect on glucose uptake. To examine whether the inhibition is regulated by transcription, we tested the effect of short-term exposure. Exposure to TBT for 1 h suppressed glucose uptake (Fig. S1, ESI†), suggesting that gene expression is not involved in the effect of TBT. Since TBT has been shown to activate transcriptional activity of peroxisome proliferator-activated receptor γ (PPARγ),[27,28] we tested the effect of the PPARγ agonist rosiglitazone on the glucose uptake. Treatment with rosiglitazone increased glucose uptake (Fig. S2, ESI†), suggesting that PPARγ is not involved in TBT-induced inhibition of glucose uptake. Furthermore, we examined the activity of hexokinase, which catalyzes the phosphorylation of glucose into glucose-6-phosphate. As shown in Fig. 2C, hexokinase activity was not significantly altered by TBT. Exposure to TA also produced similar results. These data suggest that TBT exposure decreases the amount of glycolytic metabolites *via* inhibition of glucose transport.

AMP-activated protein kinase (AMPK) is known to regulate the translocation of a glucose transporter (GLUT) to the plasma membrane.[29] We examined whether AMPK is involved in the inhibition of glycolytic systems by TBT exposure. Exposure to 100 nM TBT reduced AMPK activity (Fig. 3A). In contrast, TA had little effect on AMPK. In addition, treatment with AICAR (a potent AMPK activator) recovered the inhibitory effect of TBT on glucose uptake (Fig. 3B). To confirm the effect of AICAR, we examined the effect of constitutively active (CA) mutants of AMPK. Similar to the treatment with AICAR, overexpression of CA-AMPK recovered the inhibitory effect of TBT on glucose uptake. Overexpression of dominant-negative mutants of AMPK reduced the basal level of glucose uptake, suggesting that

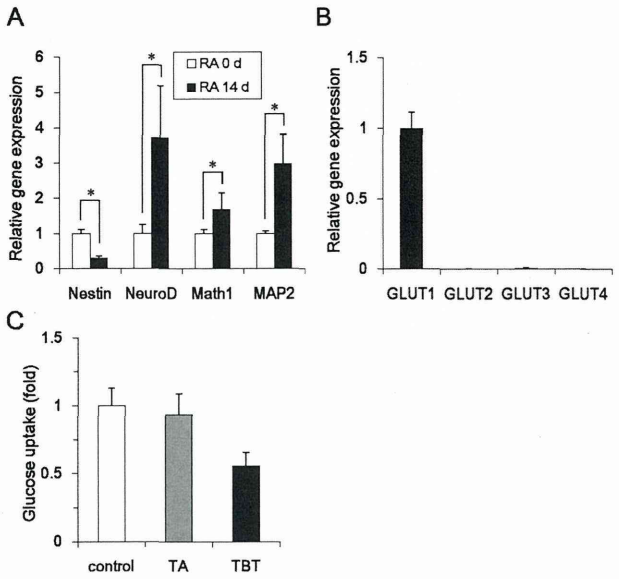

Fig. 5 Effect of neuronal induction on glucose uptake under TBT exposure in NT2/D1 cells. (A) To induce neuronal differentiation, NT2/D1 cells were treated with 10 μM RA for 14 days. The relative expression of neuronal markers (NeuroD, Math1, and MAP2) and a marker of undifferentiation (nestin) were measured by real-time-PCR. The relative changes were normalized to RPL13. (B) Expressions of members of the GLUT family were measured by real-time PCR in differentiated NT2/D1 cells. Relative changes were determined by normalizing to RPL13. (C) After exposure to 100 nM TBT for 24 h, glucose uptake was measured in differentiated cells. The fluorescence intensities of intracellularly incorporated 2-NBDG were measured and normalized to the total cellular protein levels. $*P < 0.05$.

glucose uptake is AMPK-dependent in NT2/D1 cells. Taken together, these data suggest that TBT exposure suppresses glucose uptake through the inhibition of AMPK activity.

We next examined the mechanism by which AMPK regulates glucose uptake in NT2/D1 cells. Real-time PCR analysis showed that GLUT1 was a major subtype in NT2/D1 cells (Fig. 4A). Since TBT exposure did not affect gene expression of GLUT1 (data not shown), we examined GLUT1 localization by immunohistochemistry. Expression of GLUT1 was observed at the plasma membrane and in the intracellular segment (Fig. 4B). Exposure with TBT reduced the cell surface expression of GLUT1. Treatment with AICAR recovered the inhibitory effect of TBT. To confirm these observations using microscopy, we labeled cell surface-bound GLUT1 by biotinylation of cell surface proteins (Fig. 4C). Using this approach, we determined that TBT exposure reduced the amount of cell surface-bound GLUT1. AICAR reversed this inhibitory effect of TBT. Furthermore, overexpression of GLUT1 partially recovered the TBT-induced inhibition of glucose uptake (Fig. 4D). These data suggest that TBT inhibits glucose uptake mediated by cell surface translocation of GLUT1, a process dependent on AMPK.

To examine whether the effect of TBT was selective for embryonic cells, we used NT2/D1 cells differentiated by retinoic acid.[30] Real-time PCR analysis revealed that RA-treated NT2/D1 cells showed upregulated expression of markers of differentiation (NeuroD, Math1, MAP2) and downregulated expression of a marker of undifferentiation (nestin), confirming the induction of differentiation (Fig. 5A). Real-time PCR confirmed that GLUT1 is a major subtype in the differentiated NT2/D1 cells (Fig. 5B). Furthermore, exposure to 100 nM TBT also reduced glucose uptake in differentiated NT2/D1 cells. In contrast, TA had little effect (Fig. 5C). These data suggest that TBT suppresses glucose uptake in both undifferentiated and differentiated cells.

Discussion

In the present study, we showed that the glycolytic pathway is a novel target of TBT toxicity in human embryonic carcinoma cells. We showed that TBT suppresses AMPK-dependent glucose uptake, and thereby, the amount of glucose-6-phosphate. The inhibitory effects of TBT on glycolytic systems would lead to growth arrest in the cells. Fig. 6 shows a proposed model of TBT-induced toxicity, based on the data observed in our study.

Our studies showed that treatment with 1 μM TBT resulted in the death of human embryonic carcinoma cells (Fig. 1). Consistent with these observations, previous studies have shown that micromolar levels of TBT induce apoptosis in various cells such as human amnion cells,[31] hepatocytes,[32] and neutrophils.[33] In contrast, exposure to 100 nM TBT resulted in neither growth arrest nor cell death. Therefore, we focused on intracellular metabolites as potential mediators of TBT-induced growth arrest. We found that exposure to nanomolar levels of TBT affects the intracellular metabolic balance and decreases the amount of glucose metabolites (Fig. 2). A previous report showed that the organotin compounds such as TBT might be present in human blood at nanomolar levels.[16] Glucose metabolism analysis revealed novel toxic mechanisms

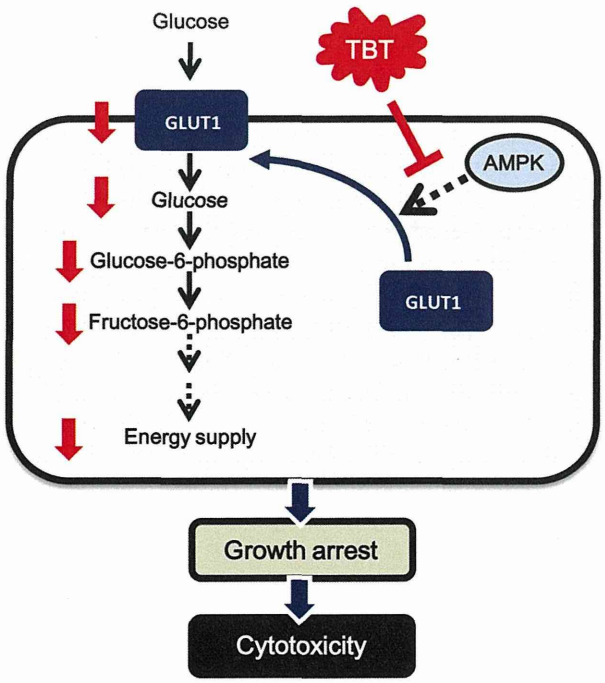

Fig. 6 Proposed model of TBT toxicity in human embryonic carcinoma cells.

for the toxicity of nanomolar levels of TBT. Thus, the glycolytic pathway might account for the unknown toxic mechanism induced by heavy metal exposure.

Our data suggest that the target molecule of TBT toxicity is GLUT1, a major subtype of GLUT in NT2/D1 cells (Fig. 4). Since the expression of GLUT1 is observed in a broad range of cell types, the toxicity of TBT may also be observed in other cells. For example, we showed that TBT reduces glucose uptake in differentiated NT2/D1 cells, which express GLUT1 (Fig. 5). Thus, it is possible that TBT induces toxicity in mature neurons *via* inhibition of GLUT function.

We showed that TBT decreases AMPK activity, one of the GLUT regulators, in NT2/D1 cells (Fig. 3). In addition, overexpression of AMPK or the AMPK activator restored the glucose uptake, confirming that AMPK is a possible target of TBT. In contrast, 500 nM TBT has been shown to increase AMPK phosphorylation in rat cortical neurons.[34] This discrepancy might be due to the concentration of TBT or different types of cells.

Several studies suggest that TBT directly interacts with target enzymes. TBT at a concentration of 10–100 nM has been shown to act as an agonist of PPARγ and the retinoid X receptor (RXR) because of its higher binding affinity compared to intrinsic ligands. Other studies reported that micromolar concentrations of TBT inhibit F1F0 ATP synthase and 11β-hydroxysteroid dehydrogenase by direct interaction.[35,36] Therefore, TBT can bind to multiple targets with broad specificity. It is possible that TBT also interacts with AMPK. On the other hand, calmodulin-dependent protein kinase II (CaMK II) and serine–threonine liver kinase B1 (LKB1) have been shown to phosphorylate AMPK and cause subsequent activation of glucose transport.[29] Furthermore, there may be an additional signaling molecule between TBT and AMPK. It remains to be elucidated how TBT regulates AMPK in embryonic carcinoma cells.

Nanomolar levels of TBT may interact with several targets in other types of cells, such as PPARγ, RXR, and α-amino-3-hydroxy-5-methylisoxazole-4-propionic acid (AMPA) receptors 2 (GluR2). Since rosiglitazone, a PPARγ agonist, increased glucose transport in NT2/D1 cells (Fig. S2, ESI†), it is unlikely that TBT inhibits glucose transport *via* PPARγ in the cells. RXR transgenic mice have been shown to exhibit an increase in GLUT1 expression in the skeletal muscles.[37] Since the expression level of GLUT1 was not changed by TBT exposure in NT2/D1 cells and the inhibitory effect of glucose uptake was observed after a 1 h treatment with TBT, it is likely that RXR is not involved in TBT-mediated alteration of glucose transport. Moreover, exposure to nanomolar levels of TBT has been reported to decrease the mRNA expression of GluR2 in cultured rat cortical neurons.[38] Although NT2/D1 cells do not express GluR2, it is possible that GluR2 may be a target in the differentiated NT2/D1 cells. Further studies are required to examine these targets other than the glycolytic pathway.

Conclusions

We found that exposure to nanomolar levels of TBT mainly targets the glycolytic systems in human embryonic carcinoma cells. Thus, glycolytic systems may be a good target for previously unknown mechanisms of toxicity induced by metal exposure at nanomolar levels.

Conflict of interest

The authors declare that there are no conflicts of interest.

List of abbreviations

AMPK	AMP-activated protein kinase
GLUT	glucose transporter
RA	all-trans retinoic acid
PPARγ	peroxisome proliferator-activated receptor γ
TA	tin acetate
TBT	tributyltin

Acknowledgements

We would like to thank Dr Rathmell and Dr Carling for providing the materials. This study was supported in part by a Health and Labour Sciences Research Grant from the Ministry of Health, Labour and Welfare, Japan (Y. Ka.), a grant from the Program for Promotion of Fundamental Studies in Health Sciences of the National Institute of Biomedical Innovation (NIBIO) (No. 09-02 to Y. Ka.), Grants-in-Aid for Scientific Research (No. 23590322 to Y. Ka. and No. 23310047 to Y. Ko.) from the Japan Society for the Promotion of Science, and a grant from the Smoking Research Foundation (Y. Ka.).

References

1 H. L. Needleman, C. Gunnoe, A. Leviton, R. Reed, H. Peresie, C. Maher and P. Barrett, Deficits in psychologic and classroom performance of children with elevated dentine lead levels, *N. Engl. J. Med.*, 1979, **300**, 689–695.

2 G. Winneke, Developmental aspects of environmental neurotoxicology: lessons from lead and polychlorinated biphenyls, *J. Neurol. Sci.*, 2011, **308**, 9–15.

3 L. G. Costa, M. Aschne, A. Vitalone, T. Syversen and O. P. Soldin, Developmental neuropathology of environmental agents, *Annu. Rev. Pharmacol. Toxicol.*, 2004, **44**, 87–110.

4 J. Dobbing, *Vulnerable periods in developing brain*, in *Appl. Neurochem.*, ed. A. N. Davison and J. Dobbing, Davis, Philadelphia, 1968, pp. 287–316.

5 P. M. Rodier, Developing brain as a target of toxicity, *Environ. Health Perspect.*, 1995, **103**(suppl 6), 73–76.

6 D. Rice and S. Barone Jr, Critical periods of vulnerability for the developing nervous system: evidence from humans and animal models, *Environ. Health Perspect.*, 2000, **108**(suppl 3), 511–533.

7 H. Asakawa, M. Tsunoda, T. Kaido, M. Hosokawa, C. Sugaya, Y. Inoue, Y. Kudo, T. Satoh, H. Katagiri, H. Akita, M. Saji, M. Wakasa, T. Negishi, T. Tashiro and Y. Aizawa, Enhanced

inhibitory effects of TBT chloride on the development of F1 rats, *Arch. Environ. Contam. Toxicol.*, 2010, **58**, 1065–1073.
8 S. Gómez-Ruiz, G. N. Kaluderović, S. Prashar, E. Hey-Hawkins, A. Erić, Z. Zizak and Z. D. Juranić, Study of the cytotoxic activity of di and triphenyltin(IV) carboxylate complexes, *J. Inorg. Biochem.*, 2008, **102**, 2087–2096.
9 L. Rocamora-Reverte, E. Carrasco-García, J. Ceballos-Torres, S. Prashar, G. N. Kaluđerović, J. A. Ferragut and S. Gómez-Ruiz, Study of the anticancer properties of tin(IV) carboxylate complexes on a panel of human tumor cell lines, *ChemMedChem*, 2012, 7, 301–310.
10 A. González, E. Gómez, A. Cortés-Lozada, S. Hernández, T. Ramírez-Apan and A. Nieto-Camacho, Heptacoordinate tin(IV) compounds derived from pyridine Schiff bases: synthesis, characterization, *in vitro* cytotoxicity, anti-inflammatory and antioxidant activity, *Chem. Pharm. Bull.*, 2009, **57**, 5–15.
11 Y. Kotake, Molecular mechanisms of environmental organotin toxicity in mammals, *Biol. Pharm. Bull.*, 2012, **35**, 1876–1880.
12 T. Noda, S. Morita, T. Yamano, M. Shimizu, T. Nakamura, M. Saitoh and A. Yamada, Teratogenicity study of tri-*n*-butyltin acetate in rats by oral administration, *Toxicol. Lett.*, 1991, **55**, 109–115.
13 A. T. Gardlund, T. Archer, K. Danielsen, B. Danielsson, A. Frederiksson, N. G. Lindquist, H. Lindstrom and J. Luthman, Effects of prenatal exposure to tributyltin and trihexyltin on behavior in rats, *Neurotoxicol. Teratol.*, 1991, **13**, 99–105.
14 Q. Li, M. Osada, K. Takahashi, T. Matsutani and K. Mori, Accumulation and depuration of tributyltin oxide and its effect on the fertilization and embryonic development in the pacific oyster, *Crassostrea gigas*, *Bull. Environ. Contam. Toxicol.*, 1997, **58**, 489–496.
15 Y. Nakatsu, Y. Kotake, K. Komasaka, H. Hakozaki, R. Taguchi, T. Kume, A. Akaike and S. Ohta, Glutamate excitotoxicity is involved in cell death caused by tributyltin in cultured rat cortical neurons, *Toxicol. Sci.*, 2006, **89**, 235–242.
16 M. M. Whalen, B. G. Loganathan and K. Kannan, Immunotoxicity of environmentally relevant concentrations of butyltins on human natural killer cells *in vitro*, *Environ. Res. Lett.*, 1999, **81**, 108–116.
17 L. Pellerin, Food for thought: the importance of glucose and other energy substrates for sustaining brain function under varying levels of activity, *Diabetes Metab.*, 2010, **36**, S59–S63.
18 K. Barnes, J. C. Ingram, O. H. Porras, L. F. Barros, E. R. Hudson, L. G. Fryer, F. Foufelle, D. Carling, D. G. Hardie and S. A. Baldwin, Activation of GLUT1 by metabolic and osmotic stress: potential involvement of AMP-activated protein kinase (AMPK), *J. Cell Sci.*, 2002, **115**, 2433–2442.
19 M. Jing, V. K. Cheruvu and F. Ismail-Beigi, Stimulation of glucose transport in response to activation of distinct AMPK signaling pathways, *Am. J. Physiol.: Cell Physiol.*, 2008, **295**, C1071–C1082.
20 B. Kunievsky, J. Pretsky and E. Yavin, Transient rise of glucose uptake in the fetal rat brain after brief episodes of intrauterine ischemia, *Dev. Neurosci.*, 1994, **16**, 313–320.
21 K. Matsumoto, S. Akazawa, M. Ishibashi, R. A. Trocino, H. Matsuo, H. Yamasaki, Y. Yamaguchi, S. Nagamatsu and S. Nagataki, Abundant expression of GLUT1 and GLUT3 in rat embryo during the early organogenesis period, *Biochem. Biophys. Res. Commun.*, 1995, **209**, 95–102.
22 P. J. Jensen, J. D. Gitlin and M. O. Carayannopoulos, GLUT1 deficiency links nutrient availability and apoptosis during embryonic development, *J. Biol. Chem.*, 2006, **281**, 13382–13387.
23 Y. Kanda and Y. Watanabe, Thrombin-induced glucose transport *via* Src-p38 MAPK pathway in vascular smooth muscle cells, *Br. J. Pharmacol.*, 2005, **146**, 60–67.
24 T. Soga, Y. Ueno, H. Naraoka, Y. Ohashi, M. Tomita and T. Nishioka, Simultaneous determination of anionic intermediates for *Bacillus subtilis* metabolic pathways by capillary electrophoresis electrospray ionization mass spectrometry, *Anal. Chem.*, 2002, **74**, 2233–2239.
25 Y. Kanda and Y. Watanabe, Adrenaline increases glucose transport *via* a Rap1-p38MAPK pathway in rat vascular smooth muscle cells, *Br. J. Pharmacol.*, 2007, **151**, 476–482.
26 N. Hiarta, Y. Sekinoa and Y. Kanda, Nicotine increases cancer stem cell population in MCF-7 cells, *Biochem. Biophys. Res. Commun.*, 2010, **403**, 138–143.
27 T. Kanayama, N. Kobayashi, S. Mamiya, T. Nakanishi and J. Nishikawa, Organotin compounds promote adipocyte differentiation as agonists of the peroxisome proliferator-activated receptor gamma/retinoid X receptor pathway, *Mol. Pharmacol.*, 2005, **67**, 766–774.
28 F. Grün, H. Watanabe, Z. Zamanian, L. Maeda, K. Arima, R. Cubacha, D. M. Gardiner, J. Kanno, T. Iguchi and B. Blumberg, Endocrine-disrupting organotin compounds are potent inducers of adipogenesis in vertebrates, *Mol. Endocrinol.*, 2006, **20**, 2141–2155.
29 D. G. Hardie, F. A. Ross and S. A. Hawley, AMPK: a nutrient and energy sensor that maintains energy homeostasis, *Nat. Rev. Mol. Cell Biol.*, 2012, **13**, 251–262.
30 S. J. Pleasure, C. Page and V. M. Lee, Pure, postmitotic, polarized human neurons derived from NTera 2 cells provide a system for expressing exogenous proteins in terminally differentiated neurons, *J. Neurosci.*, 1992, **12**, 1802–1815.
31 X. Zhu, M. Xing, J. Lou, X. Wang, W. Fu and L. Xu, Apoptotic related biochemical changes in human amnion cells induced by tributyltin, *Toxicology*, 2007, **230**, 45–52.
32 M. Grondin, M. Marion, F. Denizeau and D. A. Averill-Bate, Tributyltin induces apoptotic signaling in hepatocytes through pathways involving the endoplasmic reticulum and mitochondria, *Toxicol. Appl. Pharmacol.*, 2007, **222**, 57–68.
33 V. Lavastre and D. Girard, Tributyltin induces human neutrophil apoptosis and selective degradation of cytoskeletal proteins by caspases, *J. Toxicol. Environ. Health, Part A*, 2002, **65**, 1013–1024.

34 Y. Nakatsu, Y. Kotake, A. Hino and S. Ohta, Activation of AMP-activated protein kinase by tributyltin induces neuronal cell death, *Toxicol. Appl. Pharmacol.*, 2008, **230**, 358–363.
35 C. von Ballmoos, J. Brunner and P. Dimroth, The ion channel of F-ATP synthase is the target of toxic organotin compounds, *Proc. Natl. Acad. Sci. U. S. A.*, 2004, **101**, 11239–11244.
36 A. G. Atanasov, L. G. Nashev, S. Tam, M. E. Baker and A. Odermatt, Organotins disrupt the 11β-hydroxysteroid dehydrogenase type 2-dependent local inactivation of glucocorticoids, *Environ. Health Perspect.*, 2005, **113**, 1600–1606.
37 S. Sugita, Y. Kamei, F. Akaike, T. Suganami, S. Kanai, M. Hattori, Y. Manabe, N. Fujii, T. Takai-Igarashi, M. Tadaishi, J. Oka, H. Aburatani, T. Yamada, H. Katagiri, S. Kakehi, Y. Tamura, H. Kubo, K. N. S. Miura, O. Ezaki and Y. Ogawa, Increased systemic glucose tolerance with increased muscle glucose uptake in transgenic mice overexpressing RXRγ in skeletal muscle, *PLoS One*, **6**, e20467.
38 Y. Nakatsu, Y. Kotake Y, T. Takishit and S. Ohta, Long-term exposure to endogenous levels of tributyltin decreases GluR2 expression and increases neuronal vulnerability to glutamate, *Toxicol. Appl. Pharmacol.*, 2009, **240**, 292–298.

SCIENTIFIC REPORTS

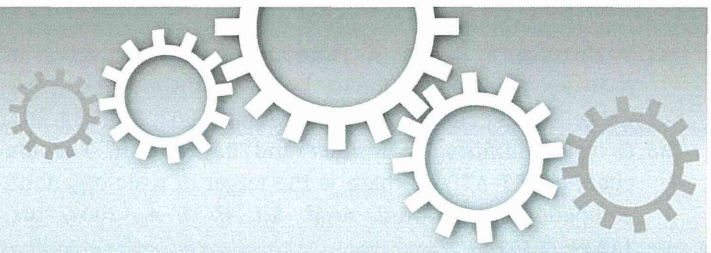

OPEN

SUBJECT AREAS:
METABOLOMICS
ENVIRONMENTAL SCIENCES

Received
17 February 2014

Accepted
15 July 2014

Published
5 August 2014

Correspondence and requests for materials should be addressed to Y.Ka (kanda@nihs.go.jp)

NAD-dependent isocitrate dehydrogenase as a novel target of tributyltin in human embryonic carcinoma cells

Shigeru Yamada[1], Yaichiro Kotake[2], Yosuke Demizu[3], Masaaki Kurihara[3], Yuko Sekino[1] & Yasunari Kanda[1]

[1]Division of Pharmacology, National Institute of Health Sciences, Tokyo, Japan, [2]Graduate School of Biomedical and Health Sciences, Hiroshima University, Hiroshima, Japan, [3]Division of Organic Chemistry, National Institute of Health Sciences, Tokyo, Japan.

Tributyltin (TBT) is known to cause developmental defects as endocrine disruptive chemicals (EDCs). At nanomoler concentrations, TBT actions were mediated by genomic pathways via PPAR/RXR. However, non-genomic target of TBT has not been elucidated. To investigate non-genomic TBT targets, we performed comprehensive metabolomic analyses using human embryonic carcinoma NT2/D1 cells. We found that 100 nM TBT reduced the amounts of α-ketoglutarate, succinate and malate. We further found that TBT decreased the activity of NAD-dependent isocitrate dehydrogenase (NAD-IDH), which catalyzes the conversion of isocitrate to α-ketoglutarate in the TCA cycle. In addition, TBT inhibited cell growth and enhanced neuronal differentiation through NAD-IDH inhibition. Furthermore, studies using bacterially expressed human NAD-IDH and *in silico* simulations suggest that TBT inhibits NAD-IDH due to a possible interaction. These results suggest that NAD-IDH is a novel non-genomic target of TBT at nanomolar levels. Thus, a metabolomic approach may provide new insights into the mechanism of EDC action.

Endocrine disruptive compounds (EDCs) have been studied extensively in environmental biology[1]. A large number of EDCs are known to cause genomic action via nuclear receptor. For example, xenoestrogens such as bisphenol A, genistein and diethylstilbestrol can bind to the estrogen receptor (ER) in the cell nucleus, followed by the alteration of gene expression[2,3]. In addition, EDCs induce the activation of non-genomic signaling pathways. For example, xenoestrogens increase intracellular calcium levels, activating eNOS and signaling cascades such as PI3K/AKT and MAPK[4–7]. Thus, both genomic and non-genomic pathways are required to understand the mechanism of EDC action.

Organotin compounds, such as tributyltin (TBT) are typical environmental contaminants and well known to cause developmental defects as EDCs. For example, TBT can cause increased fetal mortality, decreased fetal birth weights, and behavioral abnormalities in rat offspring[8,9]. Although the use of TBT has already been restricted, butyltin compounds, including TBT, can still be found in human blood at concentrations between 50 and 400 nM[10]. Several studies revealed that TBT activates retinoid X receptor (RXR) and/or peroxisome proliferator-activated receptor γ (PPARγ). These genomic transcriptional activations result in developmental effects, such as the imposex in many marine species[11–13] and the enhancement of adipocyte differentiation in mammals[14,15]. These TBT actions involve a higher binding affinity compared to intrinsic ligands at nM concentrations. In addition to the genomic effects, non-genomic action of TBT has been also reported. For example, TBT has been reported to inhibit the steroid biosynthesis pathway, which is responsible for the production of estrogen and androgen[16–18]. Another report has shown that TBT inhibits mitochondrial F1F0 ATP synthase[19]. These data were obtained at μM concentrations. Thus, the mechanism of nM concentrations of TBT has not been elucidated at a non-genomic level. In a previous study, we reported that treatment with 100 nM TBT resulted in growth arrest by targeting the glycolytic systems of the human embryonic carcinoma cell line NT2/D1[20]. Therefore, we raised the possibility that nM concentrations of TBT may target other non-genomic pathways which are involved in energy metabolism.

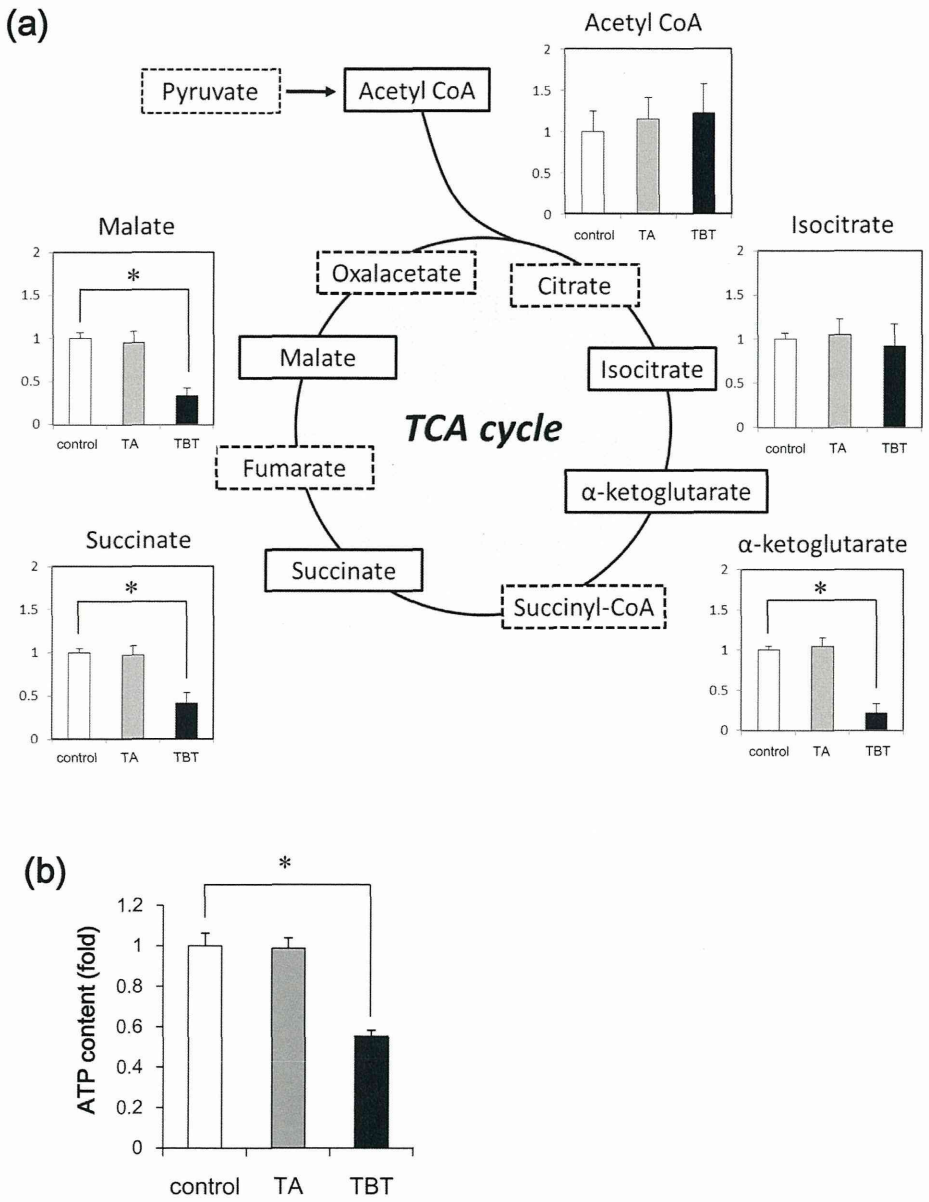

Figure 1 | Metabolomic analysis of NT2/D1 cells exposed to TBT. The cells were exposed to 100 nM TBT or TA for 24 h. (a) The levels of several metabolites, such as acetyl CoA, isocitrate, α-ketoglutarate, succinate and malate, were determined using CE-TOFMS. (b) The intracellular ATP content was determined in the lysed cells. * $P < 0.05$ compared with the corresponding control group.

In the present study, we investigated the molecular target of TBT at nM levels by comprehensive determination of the intracellular metabolites in NT2/D1 cells after TBT exposure. We found that exposure to 100 nM TBT reduced ATP production via NAD-dependent isocitrate dehydrogenase (NAD-IDH) in the cells. This NAD-IDH inhibition resulted in the reduction of the TCA cycle metabolites. In addition, TBT caused neural differentiation through an NAD-IDH-dependent mechanism. We report here that our metabolomic analysis revealed that NAD-IDH is a novel target of TBT in embryonic carcinoma cells.

Results

Metabolomic analysis of NT2/D1 cells exposed to TBT at nM levels. To investigate the non-genomic effects of a well-known endocrine disruptor TBT in human NT2/D1 embryonic carcinoma cells, we comprehensively determined intracellular metabolites using LC/MS. We found that exposure to 100 nM TBT reduced the amounts of TCA cycle components, such as α-ketoglutarate, succinate and malate (Figure 1a). The amounts of acetyl CoA and isocitrate were not changed. We also found that treatment with 100 nM TBT reduced the ATP content of the cells (Figure 1b). In contrast to TBT, exposure to the less toxic tin acetate (TA) did not affect the amount of each metabolite. These data suggest that TBT exposure decreases the amounts of TCA cycle metabolites, resulting in a reduction of ATP content.

NAD-IDH enzyme activity of NT2/D1 cells exposed to TBT at nM levels. Based on the results of the metabolomic analysis, we focused

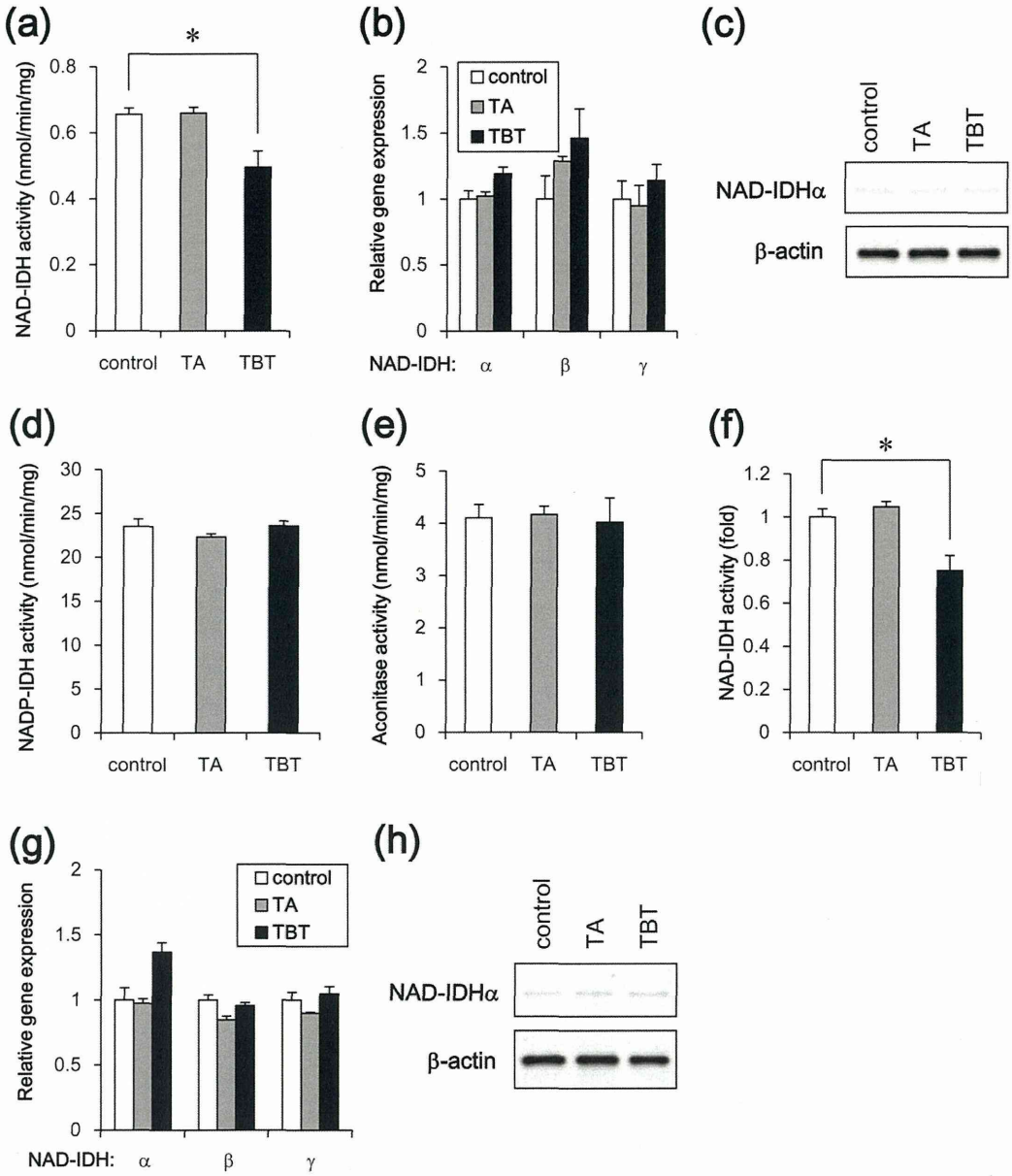

Figure 2 | Effect of TBT exposure on NAD-IDH enzyme activity in NT2/D1 cells. The cells were exposed to 100 nM TBT or TA for 24 h. (a) NAD-IDH activity was determined in the lysed cells. (b) The relative expressions of NAD-IDHα, β, and γ were measured using real-time PCR. The relative changes were normalized to the levels of RPL13. (c) The expression of NAD-IDHα protein was examined by western blot analysis using the anti-NAD-IDHα and anti-β-actin antibodies. Cropped blots were shown and the full-length blots were indicated in Supplementary Fig. 4. (d) NADP-IDH activity was determined in the lysed cells. (e) Aconitase activity was determined in the lysed cells. (f) To induce neuronal differentiation, the NT2/D1 cells were treated with 10 μM retinoic acid (RA) for 14 days. After exposure to 100 nM TBT for 24 h, NAD-IDH activity was determined in the lysed cells. (g) The relative expression levels of NAD-IDHα, β, and γ in the differentiated cells were measured using real-time PCR. The relative changes were normalized to the levels of RPL13. (h) The expression of NAD-IDHα protein was examined by western blot analysis using the anti-NAD-IDHα and anti-β-actin antibodies. Cropped blots were shown and the full-length blots were indicated in Supplementary Fig. 4. * $P < 0.05$ compared with the corresponding control group.

on isocitrate dehydrogenase, which catalyzes the conversion of isocitrate to α-ketoglutarate in the TCA cycle. Eukaryotes have different types of isocitrate dehydrogenases, such as NAD-dependent form (NAD-IDH; EC 1.1.1.41) and NADP-dependent form (NADP-IDH; EC 1.1.1.42)[21]. NAD-IDH is first rate-limiting enzyme in the TCA cycle and catalyzes an irreversible reaction, while NADP-IDH is involved in reversible reaction for biosynthesis via production of NADPH. As shown in Figure 2a, NAD-IDH activity was significantly reduced following TBT treatment. Since NAD-IDH is a heterotetramer composed of two α subunits (catalytic subunit), one β subunit and one γ subunit (regulatory subunit), we examined the expression of each subunit gene. Real-time PCR analysis showed

that the expression of the NAD-IDHα, β and γ genes was not significantly changed by TBT exposure (Figure 2b). The protein expression of catalytic α subunits was not also changed by TBT exposure (Figure 2c). TA exposure did not affect either the enzyme activity or the NAD-IDH expression. We next examined the effect of TBT on NADP-IDH. The activity of NADP-IDH was not affected by TBT exposure (Figure 2d). We further examined the activity of aconitase (EC 4.2.1.3.), which catalyzes the conversion of citrate to isocitrate in the TCA cycle. Aconitase activity was also not affected by TBT exposure (Figure 2e). Thus, these data suggest that the inhibitory effect of TBT is specific to NAD-IDH in the TCA cycle.

To investigate whether TBT cytotoxicity was caused by a genomic transcriptional regulation, we tested the effects of the protein synthesis inhibitor cycloheximide in NT2/D1 cells. Treatment with cycloheximide did not alter the inhibitory effects of TBT on NAD-IDH activity (Figure S1a) and intracellular ATP production (Figure S2a). Moreover, the PPARγ agonist rosiglitazone did not reduce NAD-IDH activity (Figure S1b) and ATP content (Figure S2b). These results suggest that transcriptional regulation is not involved in the inhibition of NAD-IDH activity by TBT.

To examine whether the effect of TBT was selective for embryonic cells, we used NT2/D1 cells that had differentiated in response to retinoic acid. We observed that TBT also inhibited NAD-IDH activity in the differentiated NT2/D1 cells (Figure 2f). Real-time PCR analysis showed that the expression of the NAD-IDHα, β, and γ genes was not significantly affected by TBT exposure (Figure 2g). The protein expression of catalytic α subunits was not also changed by TBT exposure (Figure 2h). TA exposure did not affect either the activity or the NAD-IDH expression. These data suggest that TBT reduces NAD-IDH enzyme activity regardless of the developmental stage of the embryonic carcinoma cells.

Neuronal differentiation of RA-treated NT2/D1 cells exposed to TBT at nM levels. It has been reported that ATP content decreases during the differentiation of human embryonic stem cells into neural stem cells (NSCs)[22]. Therefore, the reduction of ATP caused by TBT treatment might be involved in neuronal differentiation. Moreover, TBT has been reported to cause cell growth arrest in NT2/D1 cells[20]. Because cell growth is generally reduced during differentiation, we examined whether TBT affects the neuronal differentiation process in NT2/D1 cells. Real-time PCR analysis revealed that retinoic acid (RA)-treated NT2/D1 cells showed increased expression of the differentiation markers NeuroD and Math1, confirming that neural differentiation had occurred (Figure 3a). Furthermore, we observed that TBT exposure enhanced the expression levels of these neuronal differentiation markers. Treatment with rosiglitazone had little effect on their expression (Figure S3), suggesting that PPARγ is not involved in neuronal differentiation. Taken together, these data suggest that TBT promotes neuronal differentiation.

Effect of NAD-IDH knockdown on neuronal differentiation in RA-treated NT2/D1 cells. To further investigate whether the neuronal differentiation triggered by TBT exposure is through an NAD-IDH-dependent mechanism, we performed knockdown (KD) of NAD-IDHα, the catalytic subunit of NAD-IDH, using lentivirus-delivered shRNAs. Real-time PCR analysis showed that KD efficiency was approximately 40% (Figure 3b). Due to the partial KD of the NAD-IDHα gene, NAD-IDH activity decreased to a level (22%) comparable to its level following TBT inhibition (24%) (Figure 3c). Further reduction of NAD-IDH activity was not significantly observed after TBT exposure in the NAD-IDHα KD cells. Similar to the effect of TBT, NAD-IDHα KD also reduced the ATP content of the cells (Figure 3d), and caused cell growth inhibition (Figure 3e). Further inhibition of ATP content and cell growth was not significantly observed after TBT exposure in the NAD-IDHα KD cells, suggesting that the NAD-IDH is a possible target of TBT. In addition, we found that NAD-IDHα KD significantly upregulated the expression of the neuronal differentiation markers NeuroD and Math1 (Figure 3f). These data suggest that NAD-IDH mediates TBT-induced neuronal differentiation in embryonic NT2/D1 cells.

NAD-IDH enzyme activity in the brain of rats orally exposed to TBT at low doses. To examine whether the in vitro inhibitory effect of TBT on NAD-IDH is also observed in vivo, adult rats were orally exposed to TBT at doses of 5 and 50 mg/kg. NAD-IDH activity in the cerebral cortex was significantly reduced following exposure to both doses of TBT (Figure 4a). Real-time PCR analysis showed that the expression of the NAD-IDHα, β, and γ genes was not significantly affected by TBT (Figure 4b). The protein expression of catalytic α subunits was not also affected by TBT (Figure 4c). NADP-IDH and aconitase activities were not affected by exposure to either dose of TBT (Figure 4d and e). These data suggest that TBT inhibits NAD-IDH activity both in vitro and in vivo.

Reduction of recombinant hNAD-IDH enzyme activity in E. coli lysate treated with TBT at nM levels. To investigate the mechanism by which TBT inhibits NAD-IDH activity, we examined whether TBT possibly interacts with NAD-IDH or not. Since NAD-IDHα subunit alone has been reported to show no detectable IDH activity, we used an Escherichia coli co-expression system of recombinant human (h) NAD-IDHα,β,γ subunits[23]. As shown in Figure 5a, we confirmed the expression of α subunit of hNAD-IDH protein in the extracts of E. coli transformants using western blot analysis. To check the activity of the recombinant hNAD-IDH, we used irreversible and allosteric NAD-IDH regulators. ADP has been reported to activate NAD-IDH allosterically by lowering the Km for the substrate isocitrate[24]. As expected, ADP increased the activity of hNAD-IDH in our assay system. Conversely, Zn^{2+} has been reported to inhibit several metabolic enzymes, including NAD-IDH, in hepatocytes[25]. We confirmed that Zn^{2+} reduces hNAD-IDH activity. Then, we examined whether TBT directly inhibits hNAD-IDH activity by adding TBT to the E. coli extracts containing hNAD-IDH. Treatment with 100 nM TBT for 1 h significantly reduced the hNAD-IDH activity (Figure 5b). Treatment with TA had little effect. Taken together, these data suggest that TBT inhibits hNAD-IDH activity through its possible interaction, but again we can not be sure that it is through direct binding with the data we have.

***In silico* docking simulation analysis.** To further consider this possible interaction between TBT and hNAD-IDH, we estimate TBT accessibility into hNAD-IDH (EC 1.1.1.41) α and hNADP-IDH (EC 1.1.1.42) homodimers by homology modeling and docking studies. We show the overlaid structure of the calculated hNAD-IDHα and hNADP-IDH (Figure 6a). The ligand binding pocket of hNAD-IDHα was larger than that of hNADP-IDH (Figure 6b). In our docking simulation, TBT was able to access the hNAD-IDHα ligand-binding pocket, whereas the hNADP-IDH pocket was not spacious enough to accommodate TBT (Figure 6c and d). Thus, these studies suggest that the selective inhibition of NAD-IDH by TBT may be due to differences in the pocket volumes between hNAD-IDHα and hNADP-IDH.

Discussion

In the present study, we demonstrate that NAD-IDH is a novel non-genomic target of TBT at nM levels both in vitro and in vivo. We showed that exposure to nM concentrations of TBT reduced the activity of NAD-IDH due to its possible interaction. We also found that TBT exposure caused both inhibition of cell growth and enhancement of neuronal differentiation through its inhibitory effect of NAD-IDH.

Our data suggest that NAD-IDH is a novel target molecule of TBT action. NAD-IDH is a NAD-dependent form of IDH found in NT2/D1 cells and the rat brain (Figure 2–4). Because NAD-IDH is ubi-

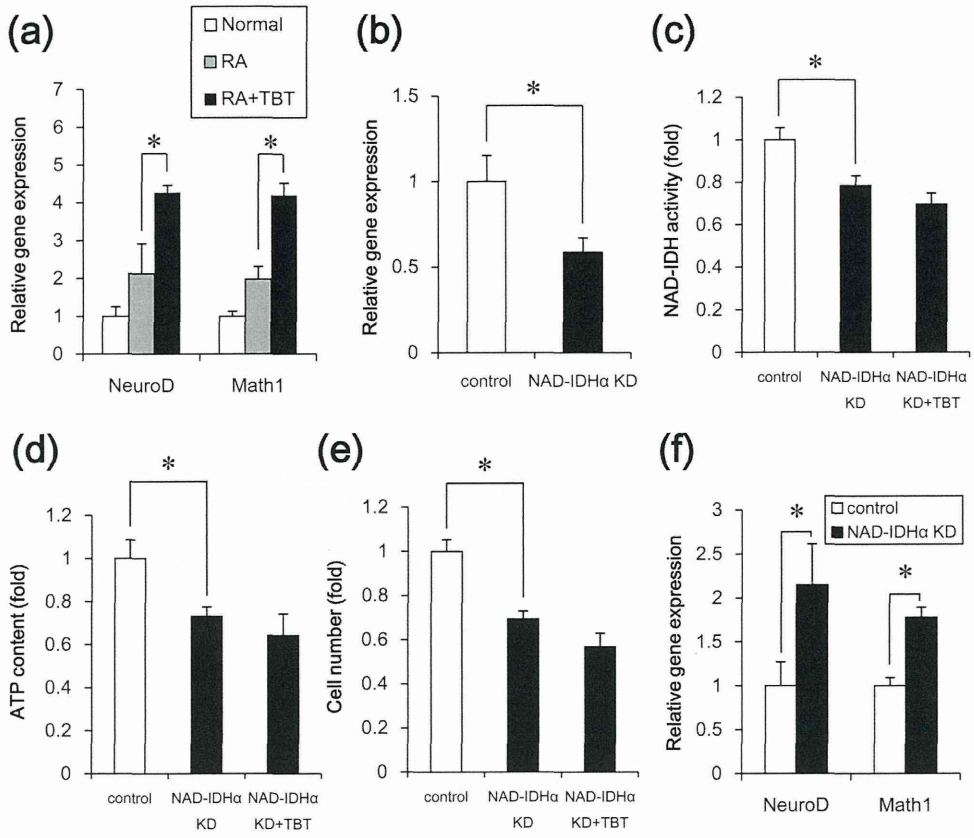

Figure 3 | Effect of TBT exposure or NAD-IDH knockdown on neuronal differentiation in RA-treated NT2/D1 cells. (a) After treatment with RA for 7 days, the cells were treated with RA in the presence of 100 nM TBT for an additional 7 days. The relative expression levels of the neuronal markers NeuroD and Math1 were measured using real-time PCR. The relative changes were determined following normalization to the levels of RPL13. (b–e) The cells were infected with lentiviruses containing a vector encoding a shRNA directed against NAD-IDHα or a scrambled sequence shRNA (control). The infected cells were subjected to selection with 0.5 μg/ml puromycin for 72 h and were then exposed to TBT at 100 nM for 24 h. (b) The relative expression of NAD-IDHα was measured using real-time PCR. The relative change in expression was normalized to the levels of RPL13. (c) NAD-IDH activity was determined in the lysed cells. (d) The intracellular ATP content was determined in the lysed cells. (e) Infected cells were seeded into 100 mm dishes and cultured for 24 h. Cell count was determined using a hemocytometer. (f) After treatment with RA for 7 days, followed by treatment with RA and the shRNA-containing lentiviruses for an additional 7 days, the relative expression levels of the neuronal markers NeuroD and Math1 were measured using real-time PCR. The relative changes were determined following normalization to the levels of RPL13. * $P < 0.05$ compared with the corresponding group.

quitously expressed, the toxicity of TBT might be observed in various cell types. Several TCA cycle enzymes have been reported to contribute to cell proliferation. For example, NADP-IDH plays a role for cell growth under hypoxic conditions in human glioblastoma cells[26]. Another study has shown that aconitase mediated cell proliferation via ATP production in human prostate carcinoma cells[27]. NAD-IDH has been shown to regulate the metabolic fluxes and the generation of ATP in the TCA cycle[28]. Therefore, it is likely that NAD-IDH is a target of TBT cytotoxicity and regulates cell growth in embryonic carcinoma cells.

In addition to cell growth inhibition, we also showed that neural differentiation is enhanced by TBT exposure or NAD-IDH inhibition (Figure 3). Consistent with our data, overexpression of NAD-IDHα has been shown to reduce neuronal differentiation and neurite outgrowth through the inactivation of MAPK phosphorylation in PC12 cells[29]. Because TBT exposure has been reported to induce neurotoxicity via ERK and p38MAPK phosphorylation in cultured rat cortical neurons[30], TBT exposure might cause cytotoxicity through the MAPK pathways. Thus, a non-genomic pathway plays a role in TBT toxicity. Indeed, the genomic target PPARγ and treatment with cycloheximide did not alter the effects of TBT (Figure S1–3). It is unlikely that transcriptional regulation is involved in NAD-IDH activity and the enhancement of neuronal differentiation. The downstream pathway of TBT-NAD-IDH should be determined in embryonic carcinoma cells.

Our data suggest that TBT regulates NAD-IDH activity through possible interaction. However, we can not conclude that it is through direct binding. Previous reports have suggested that TBT can bind to multiple target proteins, such as PPARγ, RXR, F1F0 ATP synthase and 11β-hydroxysteroid dehydrogenase (11β-HSD) type 2, with broad specificity[19,31]. For example, TBT binds the RXRα ligand-binding domain through a covalent bond between the tin atom and the Cys residue[32]. TBT also binds 11β-HSD type 2 by interacting with several Cys residues in the active site[31]. Because the ligand-binding pocket of hNAD-IDHα contains several Cys residues[33] and has enough space to accommodate TBT, TBT might bind to hNAD-IDHα via Cys residues. Future conformational analysis, including X-ray crystallography or computer simulation, and mutagenesis studies should be performed to determine whether TBT binds to hNAD-IDHα or not.

Our metabolomic analysis showed that TBT inhibited cell growth and enhanced neuronal differentiation through possible direct

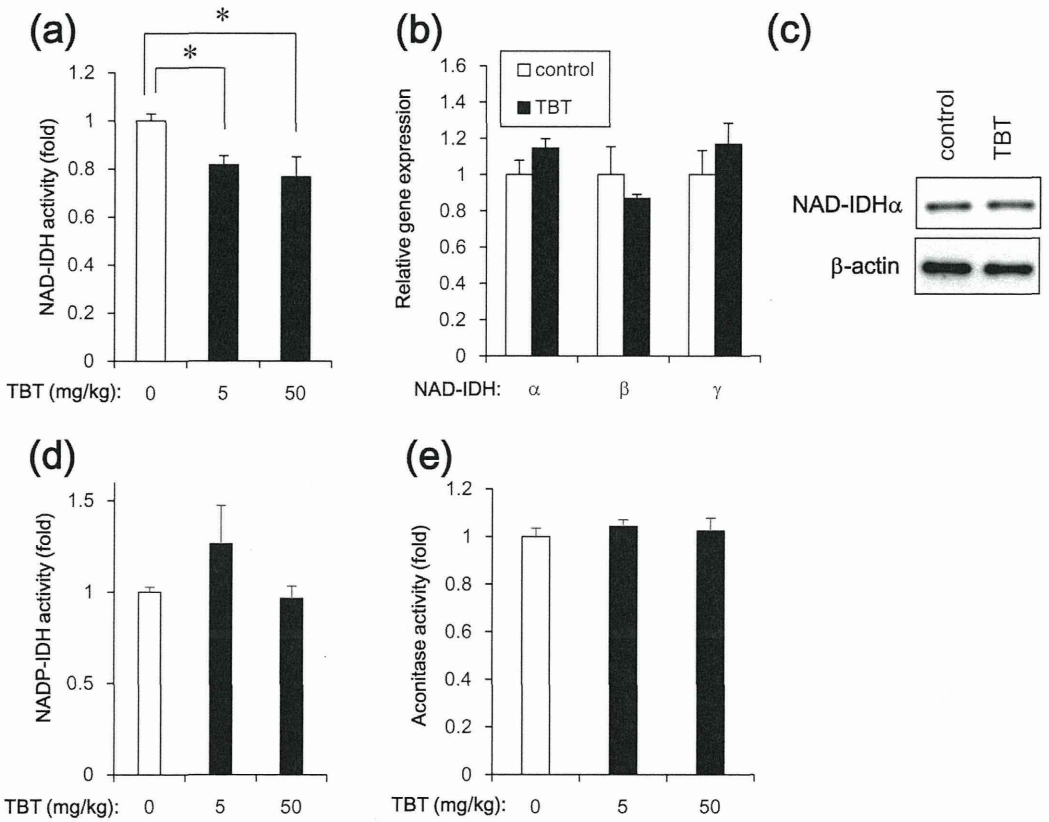

Figure 4 | NAD-IDH enzyme activity in the brain of rats orally exposed to TBT at doses of 5 and 50 mg/kg for 6 h. (a) NAD-IDH activity was determined in the brain lysates. (b) The relative expression levels of NAD-IDHα, β, and γ in rats exposed to 50 mg/kg TBT were measured using real-time PCR. The relative changes were normalized to the levels of RPL13. (c) The expression of NAD-IDHα protein was examined by western blot analysis using the anti-NAD-IDHα and anti-β-actin antibodies. Cropped blots were shown and the full-length blots were indicated in Supplementary Fig. 4. (d) NADP-IDH activity was determined in the brain lysates. (e) Aconitase activity was determined in the brain lysates. * $P < 0.05$ compared with the corresponding TBT 0 group.

inhibition of NAD-IDH activity in human embryonic carcinoma cells. Thus, comprehensive approach of non-genomic metabolic pathway might be a powerful tool to elucidate the mechanism of EDC action.

Methods

Chemicals and reagents. TBT was obtained from Tokyo Chemical Industry (Tokyo, Japan). Tin acetate (TA) and rosiglitazone were obtained from Sigma-Aldrich (St. Louis, MO, USA). All other reagents were of analytical grade and were obtained from commercial sources.

Cell culture. NT2/D1 cells were obtained from the American Type Culture Collection. The cells were cultured in Dulbecco's modified Eagle's medium (DMEM; Sigma-Aldrich) supplemented with 10% fetal bovine serum (FBS; Biological Industries, Ashrat, Israel) and 0.05 mg/ml penicillin-streptomycin mixture (Life Technologies, Carlsbad, CA, USA) at 37°C and 5% CO2. For neural differentiation, all-trans retinoic acid (RA; Sigma-Aldrich) was added to the medium twice a week at a final concentration of 10 μM.

Determination of TCA cycle metabolites. Intracellular metabolites were extracted and used for subsequent capillary electrophoresis time-of-flight mass spectrometry (CE-TOFMS) analysis, as previously described. The amounts of the metabolites were determined using an Agilent CE capillary electrophoresis system (Agilent Technologies, Waldbronn, Germany) equipped with an Agilent G3250AA LC/MSD TOF system (Agilent Technologies, Palo Alto, CA), an Agilent 1100 series isocratic HPLC pump, a G1603A Agilent CE-MS adapter kit, and a G1607A Agilent CE-electrospray ionization 53-MS sprayer kit. For system control and data acquisition, the G2201AA Agilent ChemStation software was used for CE, and the Agilent TOF (Analyst QS) software was used for the TOFMS.

Measurement of intracellular ATP levels. The intracellular ATP content was measured using the ATP Determination Kit (Life Technologies), according to the manufacturer's protocol. Briefly, the cells were washed and lysed with 0.1% Triton X-100/PBS. The resulting cell lysates were added to a reaction mixture containing 0.5 mM D-luciferin, 1 mM DTT, and 1.25 μg/ml luciferase and incubated for 30 min at room temperature. Luminescence was measured using a Wallac1420ARVO fluoroscan (Perkin-Elmer, Waltham, MA, USA). The luminescence intensities were normalized to the total protein content.

Isocitrate dehydrogenase (IDH) activity assay. IDH activity was determined using the commercial Isocitrate Dehydrogenase Activity Colorimetric Assay Kit (Biovision, Mountain View, CA, USA), according to the manufacturer's instructions. Briefly, NT2/D1 cells were lysed in an assay buffer provided in the kit. The lysate was centrifuged at 14,000 g for 15 min, and the cleared supernatant was used for the assay. NADP or NAD was used as the substrate for the NADP-IDH or NAD-IDH assay, respectively.

Real-time PCR. Total RNA was isolated from NT2/D1 cells using the TRIzol reagent (Life Technologies), and quantitative real-time reverse transcription (RT)-PCR with the QuantiTect SYBR Green RT-PCR Kit (QIAGEN, Valencia, CA, USA) was performed using an ABI PRISM 7900HT sequence detection system (Applied Biosystems, Foster City, CA, USA), as previously reported. The relative changes in the transcript amounts of each sample were normalized to the mRNA levels of ribosomal protein L13 (RPL13). The following primer sequences were used for real-time PCR analysis: human NAD-IDHα: forward, 5′-ATCGGAGGTCTCGGTGTG-3′, reverse, 5′-AGGAGGGCTGTGGGATTC-3′; human NAD-IDHβ: forward, 5′-GCCTC-AGCCGCATATCATAG-3′, reverse, 5′-GAGCAGGTGCTGAGTTCCAT-3′; human NAD-IDHγ: forward, 5′-TTAGCGGACGGAGGAATTGT-3′, reverse, 5′-CAGCCCTTCTCTGCCGT-3′; human NeuroD: forward, 5′-GGAAACGA-ACCCACTGTGCT-3′, reverse, 5′-GCCACACCAAATTCGTGGTG-3′; human Math1: forward, 5′-GTCCGAGCTGCTACAAACG-3′, reverse, 5′-GTGGTGGT-GGTCGCTTTT-3′; human RPL13: forward, 5′-CATCGTGGCTAAACAGGTAC-